UHASSELT
KNOWLEDGE IN ACTION

Maastricht University

Faculty of Medicine and Life Sciences
School for Life Sciences
Master of Biomedical Sciences

Master's thesis

Fabrication of Highly Robust Thiol-Ene Click Chemistry-Based Hydrogel Scaffold for 3D DLP Printing

Ulrike Arickx

Thesis presented in fulfillment of the requirements for the degree of Master of Biomedical Sciences, specialization Bioelectronics and Nanotechnology

SUPERVISOR :

Prof. dr. Louis PITET

MENTOR :

Mevrouw Mahsa EBRAHIMI

2022
2023

Transnational University Limburg is a unique collaboration of two universities in two countries: the University of Hasselt and Maastricht University.

UHASSELT
KNOWLEDGE IN ACTION

www.uhasselt.be
Universiteit Hasselt
Campus Hasselt:
Martelarenlaan 42 | 3500 Hasselt
Campus Diepenbeek:
Agoralaan Gebouw D | 3590 Diepenbeek

UHASSELT
KNOWLEDGE IN ACTION

Maastricht University

Faculty of Medicine and Life Sciences
School for Life Sciences
Master of Biomedical Sciences

Master's thesis

Fabrication of Highly Robust Thiol-Ene Click Chemistry-Based Hydrogel Scaffold for 3D DLP Printing

Ulrike Arickx

Thesis presented in fulfillment of the requirements for the degree of Master of Biomedical Sciences, specialization Bioelectronics and Nanotechnology

SUPERVISOR :

Prof. dr. Louis PITET

MENTOR :

Mevrouw Mahsa EBRAHIMI

Fabrication of Highly Robust Thiol-Ene Click Chemistry-Based Hydrogel Scaffold for 3D DLP Printing

Arickx U[1], Ebrahimi M[1], and Pitet L[1]

[1]Advanced Functional Polymers research group, Materials Research Institute (imo-imomec),

Universiteit Hasselt, Campus Diepenbeek, Agoralaan Gebouw F - B-3590 Diepenbeek

**Running title: 3D-DLP printing of mechanically robust hydrogels*

To whom correspondence should be addressed: Prof. dr. Louis Pitet, Email: louis.pitet@uhasselt.be

Keywords: multi-arm poly(ethene oxide); thiol-ene photoclick hydrogel; homogeneous network; network architecture; 3D DLP printing.

ABSTRACT.

Osteoarthritis (OA) affects 500 million people globally, causing joint pain and limited mobility due to articular cartilage (AC) deterioration. The limited regenerative capacity of AC, its load-bearing function, and patient-specific defects fueled research focused on customizable 3D-printed hydrogel scaffolds. Although the fabrication of complex and tough multi-network hydrogel scaffolds exists, a mechanically robust yet simple single network hydrogel scaffold is preferred. In this research, the mechanical and swelling behavior of thiol-ene photo crosslinked poly(ethene oxide) (PEO) hydrogels were investigated. Selective crosslinking of three-arm (1k) -and four-arm (2k) PEO thiol building blocks with linear (6k, 10k, 20k) -or four-arm (20k) PEO norbornene resulted in homogeneous polymer networks with different topologies. The mechanical and swelling properties were respectively investigated by non-confined uniaxial compression testing and an experimental and theoretical swelling analysis. A one-layer DLP printing experiment assessed the gelation speed. Increased branching of the building blocks improved the hydrogel's network homogeneity resulting in improved mechanical and swelling performance. Four-arm PEO (2k) thiol and four-arm PEO (20k) norbornene hydrogels could be 90% compressed without fracturing and reached E-moduli of 895±10 kPa and maximum stresses of 16.4±0.6 MPa, approximating the strength of AC. Furthermore, all four-arm thiol gels showed good printability and gelled within 2s. Although increased branching showed limited swelling, the mesh size of those hydrogels is too small for biomedical applications. This research highlights that tough yet simple hydrogels can be fabricated by tuning the network architecture.

INTRODUCTION

Articular cartilage (AC) injuries are common joint injuries among physical actives. AC is a highly specialized connective tissue of the diarthrodial joints (e.g., knee, hip, wrist, etc.) with the primary function of providing a smooth and lubricated surface for low-friction transmission of forces between adjoining bones, distributing forces and enabling optimal movement in the joint [1]. Because AC is subjected to a harsh biomechanical environment and lacks blood vessels, it has a limited intrinsic regenerative capacity [2]. If damage is left untreated, the AC wears away and exposes the underlying bone, causing friction-induced joint pains, stiffness, limited mobility, and long-term complications such as osteoarthritis [3]. Aside from pain management medication, current treatments rely on surgery based on the size of the AC defect. Restoration of AC defects smaller than two centimeters often relies on arthroscopic surgery, where they remove damaged cartilage and promote blood flow from underlying bone. For larger defects, cartilage transplants are necessary. These surgical procedures, however, are invasive, have risks for complications, and often provide only short-term relief. Hydrogel-based scaffolds, combined with or without cells, present one of the most popular future treatment strategies in cartilage defect repair [4].

Hydrogels are porous 3D polymer networks composed of hydrophilic polymer chains interconnected by chemical or physical crosslinks. With their high-water content (70-95%), hydrogels provide an environment miming the extracellular matrix (ECM). They allow critical cellular functions such as cell proliferation, migration, differentiation, and blood vessel innervation, establishing their potential in the tissue regenerative field. Meanwhile, their porous structure allows cell infiltration, diffusion of nutrients, oxygen, and other biomolecules, as well as removing toxins and metabolites [5]. The facilitation of these processes occurs solely within an optimal pore size unique to each tissue. For cartilage regeneration, pore sizes of 100-500 μm are recommended [6, 7].

Depending on how the polymer chains are interconnected, the mechanical properties of hydrogels differ significantly. Physical crosslinks rely on molecular entanglement and non-covalent interactions like hydrogen bonding, Van der Waals, and ionic interactions. Usually, they serve an energy-dissipating function and provide the hydrogels with a viscoelastic behavior. In contrast, chemical crosslinks like covalent bonds are strong irreversible interactions resulting in a gel with an elastic character [8]. However, due to their soft nature, the use of simple hydrogels for load-bearing applications is limited [9]. The three main strategies to strengthen hydrogels are nanocomposite hydrogels, dual network (DN) hydrogels, and slide ring hydrogels. Although mechanically improved hydrogels based on these strategies have been reported, their synthesis is challenging, time-consuming, and presents some limitations [10-12]. For slide-ring hydrogels, for example, pre-polymer chains threaded through cyclodextrin have to be prepared first, only then to be crosslinked. For DN hydrogels, the fabrication process requires slow sequential preparation steps. Also, finding the optimal ratio between the two networks is a tedious process, and reproducibility is mostly not guaranteed [13]. Meanwhile, some nanocomposites have poor bio adhesion and elicit a cytotoxic response [14]. So, a simpler and less laborious hydrogel design is desired. Therefore, one could prioritize the improvement of the single network's intrinsic strength by striving for homogeneity rather than introducing additional elements that may introduce complexity and multiple parameters that require control. With homogeneous networks, stress concentration on network defects is avoided and drives the network towards its optimal or ideal strength, leading to a notable improvement in its overall mechanical and swelling performance [15].

Aside from the crosslinking type, the polymer choice, polymer density, and network architecture influence the mechanical strength of hydrogels. Popular hydrogel materials include natural polymers such as alginate, chitosan, and collagen or synthetic polymers such as poly(ethylene oxide) (PEO), poly(vinyl alcohols) (PVA), polyacrylamide (PAAm) [16]. Although natural polymers possess critical biological functions like cell adhesion and biodegradation, synthetic hydrogels can be photopolymerized, and their mechanical, architectural, and chemical composition can be tuned [16-18]. Especially PEO, which is still being studied intensively, has many advantages. PEO is highly hydrophilic, allowing for good water and nutrient transport, and is biocompatible and non-immunogenic [18, 19]. However, due to their hydrophilicity, associating PEO hydrogels with biological, aqueous environments cause them to swell, a feature usually not desired for tissue engineering applications. Undeniably, swelling is associated with volume expansion. This not only deteriorates the mechanical strength of the hydrogels but can also oppress or damage the surrounding tissues when used in vivo, largely limiting their application [20-22]. Therefore, effectively controlling the swelling behavior of hydrogels by altering the hydrogel architecture (network structure and chemical composition) is an important aspect in the search for hydrogels with applications for confined tissue engineering.

Nevertheless, the main advantage of PEO lies in its chemical versatility. PEO exists in linear or branched (multi-arm) structures, resulting in a wide range of potential network topologies. The hydroxyl groups terminating PEO can be converted into other functional groups such as thiols, methyloxyls, carboxyls, amines, etc. [23]. The end-groups can be the same or different, providing different handles for hydrogel formation or bioconjugation for enhanced bioactivity. Many different PEO hydrogel synthesis methods exist, such as crosslinking through ionizing radiation, free radical polymerization, condensation reactions, Michael-type addition reactions, and click-chemistry [24]. Thiol-ene photo-click chemistry, a form of click chemistry, holds great potential for fabricating hydrogels in tissue engineering applications [25, 26]. Here selective reactions between thiols and alkenes are initiated by low photoinitiator concentrations and UV light. Employing photopolymerization offers several advantages, including flexible operation and spatiotemporal control over hydrogel formation. This precise control allows for the manipulation of network architecture, enabling directional growth and growth of specific cell types within the hydrogel scaffold [27, 28]. Moreover, thiol-ene reactions offer bio-orthogonality, ensuring minimal cytotoxicity and preserving the bioactivity of encapsulated cells. These reactions occur under mild conditions, such as physiological pH and low photoinitiator concentrations, promoting excellent biocompatibility. Additionally, thiol-ene reactions exhibit high conversion rates and are not oxygen inhibited, resulting in extremely fast (seconds vs. minutes) gelation [29, 30]. The gelation speed of the hydrogel can be influenced by altering the type of thiol or alkene used. As a result, norbornenes, which are strained cyclic alkenes known for their high reactivity, are commonly employed as ene moieties in thiol-ene chemistry [30].

Thiol-norbornene photo-induced fast gelation lends itself to cutting-edge 3D printing applications. 3D printing techniques can be divided into two major groups: ink-based 3D printing and light-based 3D printing. In ink-based 3D printing, such as extrusion or ink-jet

printing, pre-hydrogel solution (with or without cells) is deposited on a building plated by a robotically controlled printing head. Light-based 3D printing methods, such as stereolithography (SLA) printing and digital light processing (DLP) printing, operate on a light-guided printing process [15, 31, 32]. In this process, a two-dimensional layer of resin is cured within a reservoir using controlled light while a movable platform moves to print the subsequent layer. This sequential layering of cured resin ultimately generates a three-dimensional structure. Ink-based 3D printing presents significant disadvantages such as slow operation due to line-by-line or point-by-point printing, difficult processability due to low viscosity of pre-hydrogel solutions, nozzle clogging, and presence of shear forces that could damage encapsulated cells [15, 33]. Light-based printing methods, particularly DLP printing, offer significant advantages for printing with photocurable hydrogels. In DLP printing, the movable platform is positioned at the top, while a UV light projector is placed at the bottom. This setup enables the projection of a z-stacked image, layer by layer, onto the resin on the platform. After each layer is printed, the platform moves upward, allowing for the printing of the next layer. This process continues until a complete 3D structure is achieved. Due to its layer-by-layer printing approach, DLP printing effectively reduces manufacturing time. Additionally, DLP printing exhibits high fidelity, enabling rapid fabrication of hydrogel scaffolds with resolutions ranging from 1 to 100 µm. The inverted printing setup of DLP printing helps prevent unwanted swelling that may occur when the printed structure is soaked in the resin [15, 34]. However, to maintain the shape fidelity of the printed scaffold, fast crosslinking reactions are necessary. Therefore, DLP printing is associated with fast crosslinking chemistries, like thiol-ene reactions, to ensure the printed hydrogel scaffold maintains its intended shape [35, 36].

This study aims to create a rapid-curing 3D DLP printable PEO hydrogel scaffold that possesses the required mechanical strength and minimal swelling needed for AC regeneration. Instead of employing complex strengthening techniques, our focus is on enhancing the inherent strength of PEO by improving its network homogeneity. Additionally, we aim to examine the impact of various network topologies on the hydrogel's mechanical strength and swelling behavior. To achieve this, we functionalize linear (6k, 10k, 20k) PEO building blocks, as well as three-arm (1k) and four-arm (2k) PEO building blocks, with thiol and norbornene groups. This enables the fabrication of homogeneous, photo-click curable, fast gelating, and highly organized PEO hydrogels with various network architectures. Their mechanical performance and resistance to swelling will be assessed through uniaxial non-confined compression tests, along with experimental and theoretical swelling analyses. Furthermore, the printability and gelation speed of these hydrogels was assessed by conducting a one-layer DLP printing experiment.

EXPERIMENTAL PROCEDURES

Materials – linear poly(ethene oxide) (PEO) 10kg/mol, 20kg/mol (Sigma Aldrich); three-arm PEO 1kg/mol (Merck); four-arm PEO 2kg/mol (Merck); four-arm PEO 20kg/mol (JenKem Technology); 3-Mercaptopropionic acid 99% (MPA) (Thermo Scientific); Toluene (Thermo scientific), Sulphuric acid (H_2SO_4) 95% (VWR chemicals); Diethyl ether 99.5% (Thermoscientific); Dichloromethane (DCM) 99.8% (Thermoscientific); magnesium sulfate ($MgSO_4$) 99% extra pure (ARCOS organics); Tris(2-carboxyethyl)phosphine Hydrochloride (TCEP-HCl) (TCI Europe); 5-norbornene-2-carboxylic acid isomer 97%, (Thermoscientific); N'-N'-Dicyclohexylcarbodiimide (DCC) 99% (Arcos organics); 4-Dimethylaminopyridine (DMAP) 99% (Arcos organics); pyridine anhydrous max. 0.003% water (VWR chemicals); Lithium phenyl-2,4,6-trimethylbenzoylphosphinate (LAP) (TCI Europe)

Synthesis of thiol-and norbornene terminated PEO precursors

Internal polymer architecture influences the mechanical and swelling properties and the gelation speed of hydrogels. Therefore, the PEO network's crosslinking density and complexity were varied by synthesizing multi-armed thiol- and norbornene-terminated PEO precursor molecules of different lengths.

Synthesis of three-arm PEO thiol 1k - three-armed PEO was thiol end-functionalized using the fisher esterification method. The protocol was adapted from Macdougall et al., 2017. Hydroxyl-terminated PEO (1000 g/mol, 10 mmol) was suspended in 80 mL of toluene. Four drops of concentrated H_2SO_4 were added. While stirring, the solution was heated to 80 °C. Once clear, MPA (2x OH, 30 mmol) was added, and the temperature was increased to 130 °C. The water condensate, a byproduct of the reaction, was collected using the Dean-Stark apparatus, and the toluene was removed using the rotary evaporator (45 °C, 77 mbar). Next, the remaining product was dissolved in 30 mL DCM. Afterward, four to five washing steps with $NaHCO_3$ and Brine, each 20 mL, were performed and ended with 7 washes with TCEP-HCl (23.3 µM). The solution was dried using $MgSO_4$. The remaining solvent was evaporated using the rotary evaporator (45 °C, 500 mbar).

Synthesis of four-arm PEO thiol 2k – four-arm 2k PEO was norbornene end-functionalized as described above. However, the equivalent MPA (4x OH, 40 mmol) was altered related to PEO (2000 g/mol, 5 mmol).

Synthesis of linear PEO norbornene 6k – Two-armed PEO was norbornene functionalized using the Steglich esterification method. The protocol was adapted from Shih H. et al., 2012. Then, 5-norbornene-2-carboxylic acid (10x OH, 33.2 mmol) and DCC (5x OH, 16.6 mmol) reacted in 20 mL DCM (room temperature, 1h) and was afterward filtered through a fritted funnel. Separately, hydroxyl-terminated PEO (6000 g/mol, 1.66 mmol), DMAP (1x OH, 3.32 mmol), and pyridine (10x OH, 33.2 mmol) were dissolved in 25 mL DCM. Hereto, the filtrate was added in a dropwise manner. After a 24h reaction on ice, the product was washed three times with saturated $NaHCO_3$ and once with Brine. Next, the solution was dried using two spoons of $MgSO_4$. The product was precipitated twice in cold dimethyl ether (10x excess) and filtered through a fritted funnel, and vacuum dried overnight.

Synthesis of linear PEO norbornene 10k – Two-armed PEO was norbornene end-functionalized as described above. However, the equivalent reaction products related to PEO (10 000 g/mol, 1 mmol) hydroxyl groups were altered: 5-norbornene-2-carboxylic acid (15x OH, 30 mmol), DCC (7.5x OH, 15 mmol), DMAP (1.5x OH, 3 mmol) and pyridine (15x OH, 30 mmol).

Synthesis of linear PEO norbornene 20k – Two-armed PEO was norbornene end-functionalized as described above. However, the reaction time on ice was 48h, and the equivalent reaction products related to PEO's (20 000 g/mol, 0.5 mmol) hydroxyl groups were altered: 5-norbornene-2-carboxylic acid (20x OH, 20 mmol), DCC (10x OH, 10 mmol), DMAP (2x OH, 2 mmol) and pyridine (20x OH, 20 mmol).

Synthesis of four-arm PEO norbornene 20k – Four-armed PEO was norbornene end-functionalized as described above. The reaction time was 24h. However, the equivalent reaction products related to PEO's (20 000 g/mol, 0.5 mmol) hydroxyl groups were altered: 5-norbornene-2-carboxylic acid (10x OH, 20 mmol), DCC (10x OH, 10 mmol), DMAP (2x OH, 2 mmol) and pyridine (20x OH, 20 mmol).

Hydrogel synthesis

Different compositions of hydrogels were formed by photo-crosslinking linear (6k, 10k or 20k) or four-arm (20k) norbornene functionalized PEO (6k, 10k or 20k) and three- or four-arm thiol functionalized PEO (S1). The gels were formulated using a [SH]:[NB] ratio of 1:1 and had a polymer content of either 20 wt% or 25 wt%. Separately, the macromers were dissolved in distilled water. LAP (0.3 wt% for 3-arm SH and 0.05 wt% for 4-arm SH relative to end volume) was added to the thiol functionalized PEO. The resulting solutions were mixed, injected into disc-shaped molds (151 µL), and cured using UV light (365nm) for 10 minutes (S2). The hydrogels were obtained by the removal of the mold. Each hydrogel was named related to the number of arms on the thiol (SH) or norbornene (NB) precursor. The subscript denotes the polymer content, functional group, and molecular weight of the polymer. As an example, $P_{20}4_{SH2k}$-2_{NB6k}, is a 20 wt% PEO based-hydrogel from a four-arm thiol at 2 kg/mol crosslinked with a linear norbornene at 6 kg/mol (Figure 1).

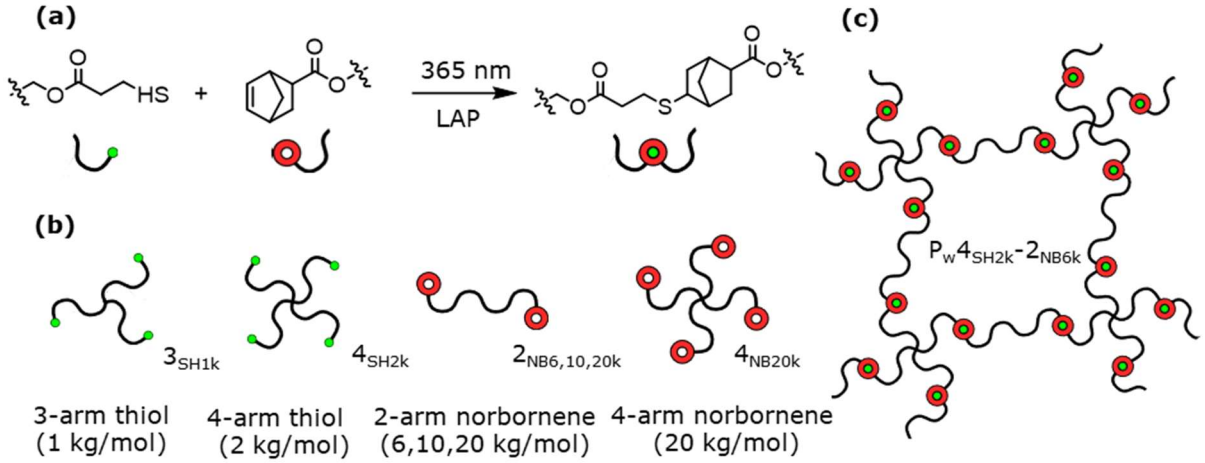

Figure 1: Overview of synthesis strategy for PEO hydrogels with various network architectures. (a) Radical-mediated thiol-ene photo click reaction between thiol and norbornene functionalized PEO. (b) Schematic representation of functionalized PEO building blocks used for hydrogel synthesis. (c) Schematic representation of exemplary hydrogel network. Figure adapted from Macdougall et al., 2017.

Swelling analysis

Next, the swelling behavior of the different hydrogel compositions, shown in S1, was analyzed. After overnight drying in the vacuum oven at 50°C and 0 bar, three replicas of each gel composition were swollen in distilled water until equilibrium was reached. The degree of swelling (DOS_{eq}) (eq. 1) and equilibrium water content (EWC) (eq. 2) were calculated using the mass of the gels after drying and the mass of the swollen gel at equilibrium.

$$DOS_{eq}\ (\%) = \frac{m_{swollen} - m_{dry}}{m_{dry}} * 100 \qquad (1)$$

$$EWC\ (\%) = \frac{m_{swollen} - m_{dry}}{m_{swollen}} * 100 \qquad (2)$$

With $m_{swollen}$, the mass of the swollen gel and m_{dry} the mass of the gel after vacuum drying.

Based on the equilibrium swelling data, Flory-Rehner calculations were used to determine the number average molecular weight between crosslinks ($\overline{M_c}$), crosslinking density, mesh size, and volume swelling ratio ($Q_{m\ eq,\ actual}$) for each hydrogel composition (S3). Flory-Rehner equation (eq. 3).

$$\frac{1}{\overline{M_c}} = \frac{2}{\overline{M_n}} = \frac{\frac{\bar{v}}{V_1}(\ln(1 - v_2) + v_2 + x_1 v_2^2)}{v_2^{\frac{1}{3}} - \frac{v_2}{2}} \qquad (3)$$

With $\overline{M_n}$, the number average molecular weight of the un-crosslinked hydrogel (theoretical molecular weight of the polymer between crosslinks), V_1 the molar volume of the solvent (18 cm^3/mol for water), v_2 the polymer volume fraction in the equilibrium swollen hydrogel, $\bar{v}$ the specific volume of the polymer, x_1 and the polymer-solvent interaction parameter (0.426 for PEO-water) [37, 38].

The perfectly crosslinked thiol-ene network without defects was estimated by means of hydrogel equilibrium. The theoretical $\overline{M_c}$ was determined considering the molecular weight of the macromer building blocks and the number of reactive functionalities (S4).

All calculations were based on averages of triplicate measurements.

Mechanical testing

The compression tests on the different compositions of hydrogels shown in S1, prepared using the molds shown in S2, were performed using a Shimadzu autograph AGS-x tensile tester equipped with a 500N or 5kN load cell. The gels were compressed until 90% strain with a velocity of 1 mm/s. Trapezium X was used as data processing software. The elastic modulus (E) was determined from the stress-strain curve of the compression test as the slope between 5% and 25% strain. The toughness, or work to fracture, was determined as the area under the curve.

DLP 3D printing

All the 3D DLP printing experiments were performed using the 20 and 25 wt% 4_{SH2k}-$2_{NB6,\ 10,20k}$ resin as described in the "Hydrogel synthesis" section.

The gelation time was gauged by performing a one-layer experiment using the DLP LightCrafter 6500 printer and corresponding DLPlcr6500 software. Here 600 µL resin was applied on ¾th of a macroscopic glass slide, on which eight identical squares (8x8 mm), one by one, were projected by a 405 nm laser. UV exposure time was varied (9s-2s) per square, starting at 9s and decreasing with 1s increments. The dark time between each projection was set at 1s, and the voxel depth equaled 4.

RESULTS & DISCUSSION

Synthesis of thiol-and norbornene terminated PEO precursors.

To fabricate thiol-norbornene photo crosslinked PEO hydrogels with different network topologies, three (1k) and four-arm (2k), and linear (6k, 10k, and 20k) and four-arm PEO building blocks were thiol (-SH) and norbornene (-NB) functionalized respectively (Figure 2). The degree of functionalization was analyzed using ^{1}H-NMR spectroscopy; all peaks in the spectrum are readily assigned to their corresponding hydrogens. The conversions were calculated based on the chemical shifts of the hydrogens next to the end groups before and after functionalization. To eliminate repetition, the focus will be on one representative molecule of thiol-functionalized PEO, four-arm (2k), and one representative molecule of linear norbornene-functionalized PEO, 6k. The characterization of the linear PEO norbornene (10k and 20k) and three-arm thiol (1k) can be found in the supplementary information (S5).

Thiol-functionalized PEO - In the case of thiol-functionalized PEO, the hydrogens (2H per arm) adjacent to the terminal hydroxyl (-OH) of the PEO underwent a chemical shift from δ 4.42-4.46 to δ 4.23-4.27 after the functionalization reaction (Figure 2a). For four-arm PEO (2k) thiol, the integration of the aforementioned peaks revealed that 99% of the hydroxyl groups have been transformed into thiol functionalities. The final product obtained after functionalization was a viscous liquid and the reaction yield was 85%.

Norbornene functionalized PEO - In case of norbornene functionalization of PEO, the hydrogens (2H per arm) adjacent to the terminal hydroxyl (-OH) of the PEO underwent a chemical shift from δ 4.42-4.46 to δ 4.12-4.26 after the functionalization reaction (Figure 2b).

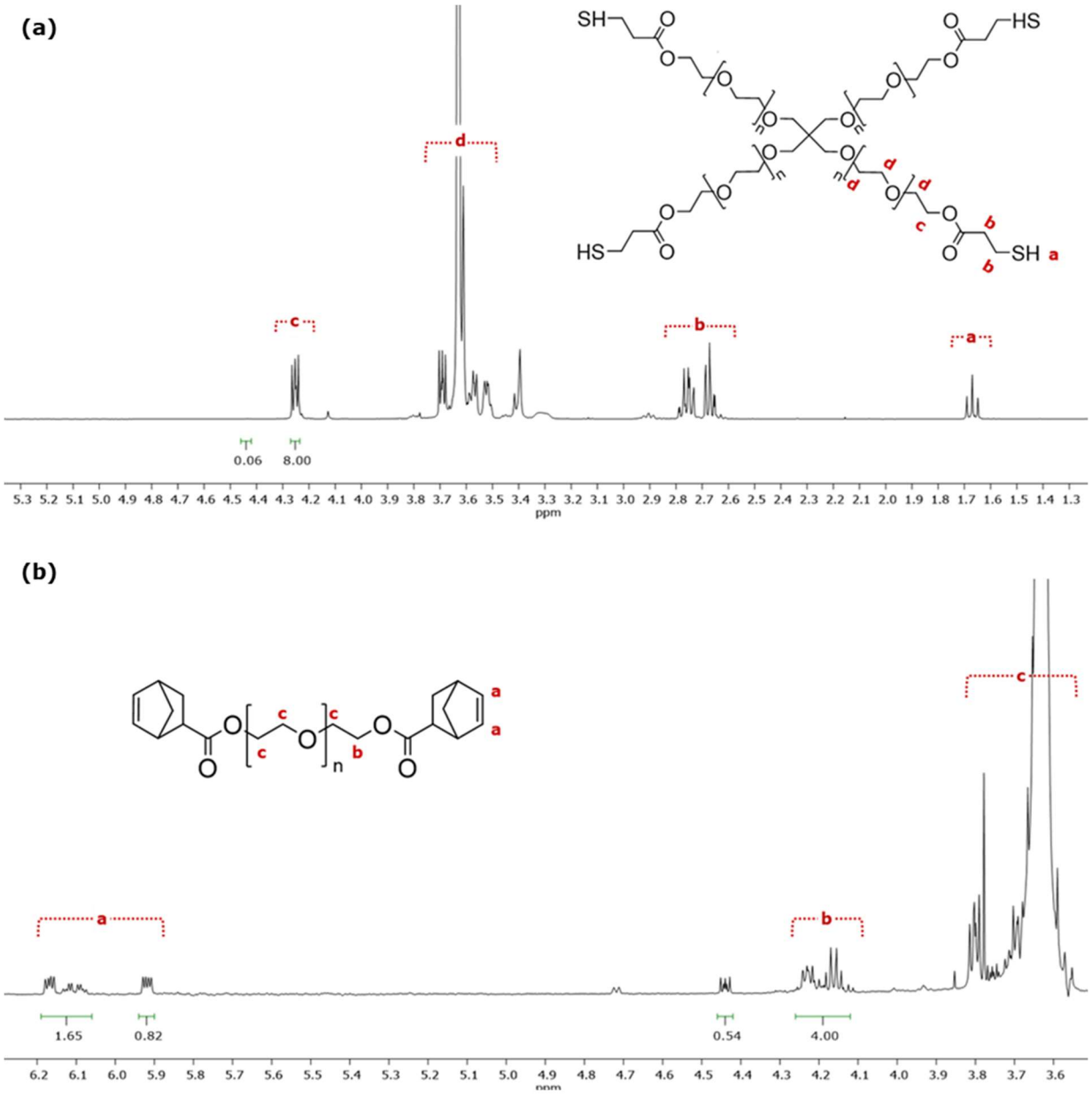

Figure 2: **^{1}H-NMR of functionalized polyethylene oxide (PEO).** ^{1}H-NMR (500 MHz, $CDCl_3$) shows quantitative thiol and norbornene end-functionalization of PEO based on comparing the theoretically expected protons next to the functionalized end-groups to those of the unfunctionalized PEO. (a) Four-arm PEO thiol (2k), 99% conversion. δ 4.23 – 4.27 (protons next to thiol functionalized end-group, 2H per arm), δ 4.42 – 4.46 (protons next to unfunctionalized hydroxyl PEO end-group, 2H per arm). (b) Linear PEO norbornene (6k), 87% conversion. δ 4.12 – 4.26 (protons next to norbornene functionalized end-group, 2H per arm), δ 4.42 – 4.46 (protons adjacent to unfunctionalized hydroxyl PEO end-group, 2H per arm), δ 6.19 – 5.90 (alkene protons from norbornene, 2H per arm).

For linear PEO (6k) norbornene, the integration of the aforementioned peaks revealed a conversion efficiency of 87%. 5-norbornene-2-carboxyllic acid, corresponding to δ 4.7, could not be removed. The final product obtained after functionalization was a white powder, and the reaction yield was 80%.

Swelling test

The effect of altering the network properties (network architecture, polymer content) on the swelling behavior of hydrogels was investigated. Hydrogels with different combinations of thiol and norbornene terminated PEO building blocks, 20 and 25 wt% polymer, were swollen until equilibrium. From this, the degree of swelling (DOS_{eq}), mesh size (ζ), crosslinking density (ρ_c), equilibrium water content (ECW), and the actual mass swelling ratio ($Q_{m\ eq,\ actual}$) were calculated (Table 1). Additionally, the theoretical mass swell ratios ($Q_{m\ eq,\ ideal}$) for each gel composition were calculated.

The swelling data shows a general trend; hydrogel networks with a low crosslinking density swell more than those with a high

crosslinking density. Focusing on the four-arm thiol 20 wt% gels ($P_{20}4_{SH2k}$-2_{NBxk}), we see that increasing the length of the linear norbornene crosslinker improves swelling. In detail, the DOS_{eq} increases from 1313±21 for 6k, 1946±23 for 10k, to 2340±64 for 20k. Accompanied by this swelling, is the decrease in crosslinking density. Specifically, from 361±1.74 to 225±0.62 to 125±0.99, for 6k, 10k and 20k respectively. Although the three-arm thiol 25 wt% and four-arm thiol 20 wt% gels show improved swelling when increasing the molecular weight of the linear crosslinker, this is not the case for all gels. The DOS_{eq} of 20k is lower compared to that of the 10k in both the three-arm 20 wt% and four-arm 25 wt% gels. Next, the effect of the polymer content on the swelling is investigated. For the majority of the gels, the 25 wt% formulations swell more than their 20 wt% equivalents. However, this is not the case for the three-arm 6k, four-arm 20k, and four-arm norbornene gels. Lastly, it was observed that increasing the number of arms of the PEO building blocks decreases the water uptake, seen as a decrease in DOS and EWC: 3SH-2NB > 4SH-2NB > 4SH-4NB. Also, the difference between the $Q_{m\ eq,\ actual,}$ and $Q_{m\ eq,\ ideal}$ decreases with increasing branching of the PEO building blocks. Literature has shown that equilibrium swelling ratios are independent of LAP concentration [39]. Therefore, differences in swelling behavior of the three-arm thiol gels, made with 0.3 wt% LAP, and four-arm thiol-linear norbornene gels, made with 0.05 wt% LAP, cannot be attributed to this.

For uncharged hydrogels, the main force driving swelling is the affinity of the solvent, here water, for the network material (solvent-polymer interaction). When water enters the network, first hydrophilic and second hydrophobic groups on the polymer chains are hydrated. This primary and secondary bound water, respectively, weakens the intermolecular interactions between polymer chains, allowing more water inflow. Finally, as more bulk or free water fill the porous space of the network, polymer chains go from a relaxed and coiled conformation into an elongated and stretched conformation. When the outward force resulting from water inflow equals the inward retractive force of the elastic polymer chains, equilibrium is reached, and the hydrogel stops swelling [21]. This phenomenon is described by the Flory-Rehner theory as the change in free energy as a result of the polymer-solvent mixing and the energy stored in elastically active polymer chains: $\Delta G = \Delta G_{mix} + \Delta G_{elastic}$. At equilibrium, ΔG equals zero, and are ΔG_{mix} and $\Delta G_{elastic}$ equal but opposite. The swelling of hydrogels can also be described in terms of crosslinking density (ρ_c), polymer volume fraction (v_2), and solvent-polymer interaction (χ_{12}) illustrated in the Flory-Rehner equation (eq. 2)[21, 40, 41]

Polymer networks with low crosslinking densities swell more than highly crosslinked networks [21, 42-45]. Crosslinking density is described as the inverse of the molecular weight between crosslinks (M_c). Therefore, increasing the Mc results in a more porous network allowing more water to enter [41, 44, 46]. In table 1 this effect is illustrated. Here, the theoretically determined mass swelling ratio ($Q_{m\ eq,\ ideal}$) increases with increasing lengths of linear crosslinker (6k to 20k). However, comparing the experimentally obtained $Q_{m\ eq,\ actual}$ of $P_{20}3_{SH1k}$-2_{NB10k} to $P_{20}3_{SH1k}$-2_{NB20k}, and $P_{25}4_{SH2k}$-2_{NB10k} to $P_{25}4_{SH2k}$-2_{NB20k}, this trend is not visible. Here, the 10k crosslinker gels swell more compared to their 20k equivalent, even though the 10k's theoretical crosslinking density is higher. This seemingly unexpected result is explained by the increased experimentally determined crosslinking density for the 20k rather than the 10k. Since network non-idealities facilitate swelling, this deviation from the theoretically expected result was likely due to network defects caused by faulty hydrogel synthesis or post-fabrication damage [21, 46]. Especially the three-arm thiol gels made with the 20k linear crosslinker were extremely soft, causing them to brake during mold removal. Since the four-arm gels had no such issue, the results were probably the result of pipetting or mixing mistakes during the synthesis of the pre-hydrogel solution.

The polymer volume fraction (v_2) is the ratio of volume taken by the polymer and the total volume of the swollen hydrogel. General findings in the literature show that increasing the polymer content of the as-prepared hydrogel results in a decrease of the polymer volume fraction, indicating enhanced swelling [43, 45, 47, 48]. A similar trend is seen for most of the swelling results obtained is this work. For the gels made with the same thiol crosslinker, we see that the 20 wt% gels made with the 20k norbornene crosslinker swell more than their 25 wt% equivalent, contradicting the aforementioned statement. However, literature suggests an alternative explanation. Because of the high length norbornene crosslinker, the possibility of forming chain entanglements increases [49].

Aside from the chemically crosslinking points, the mobility of the polymer chains between these points is now also restricted by these physical entanglements, limiting water absorption. Therefore, it seems that polymer content-based swelling is an interplay of two counteractive factors, the positive effect of solvent-polymer mixing and the negative effect of chain entangling. Nevertheless, for each hydrogel composition, there will be a value for

Table 1: Swelling data of PEO hydrogels (20 and 25 wt%) with different network architectures

Hydrogel[a]	Degree of swelling (DOS_{eq};%)	Mesh size (ζ; nm)[b]	Crosslinking density (ρ_c; mM)[b]	Equilibrium water content (EWC;%)	$Q_{m\ eq,\ actual}$	$Q_{m\ eq,\ ideal}$[c]
$P_{20}3_{SH1k}$-2_{NB6k}	2054±37	10.3±0.07	342±0.85	95.3±0.08	21.5±0.4	9.2
$P_{20}3_{SH1k}$-2_{NB10k}	3472±37	15.4±0.06	212±0.19	97.2±0.03	35.7±0.2	11.4
$P_{20}3_{SH1k}$-2_{NB20k}	3115±22	20.0±0.06	119±0.16	96.9±0.02	32.2±0.4	15.7
$P_{25}3_{SH1k}$-2_{NB6k}	1311±16	8.5±0.05	375±1.31	92.9±0.08	14.5±0.5	9.2
$P_{25}3_{SH1k}$-2_{NB10k}	3685±46	15.7±0.07	212±0.21	97.3±0.03	37.2±0.2	11.4
$P_{25}3_{SH1k}$-2_{NB20k}	3898±16	21.8±0.04	115±0.06	97.5±0.01	40.0±0.2	15.7
$P_{20}4_{SH2k}$-2_{NB6k}	1313±21	8.7±0.06	361±1.74	92.9±0.11	14.1±0.2	9.3
$P_{20}4_{SH2k}$-2_{NB10k}	1946±23	12.5±0.06	225±0.62	95.1±0.06	20.5±0.2	11.4
$P_{20}4_{SH2k}$-2_{NB20k}	2340±64	17.7±0.22	125±0.99	95.9±0.11	24.4±0.6	15.6
$P_{25}4_{SH2k}$-2_{NB6k}	1656±13	9.6±0.03	341±0.54	94.3±0.04	17.6±0.1	9.3
$P_{25}4_{SH2k}$-2_{NB10k}	2202±6	13.1±0.02	219±0.12	95.7±0.01	23.0±0.1	11.4
$P_{25}4_{SH2k}$-2_{NB20k}	2162±9	17.0±0.03	128±0.17	95.6±0.02	22.6±0.1	15.6
$P_{20}4_{SH2k}$-4_{NB20k}	1236±1	12.6±0.01	164±0.14	92.5±0.01	13.4±0.0	11.4
$P_{25}4_{SH2k}$-4_{NB20k}	1048±7	11.1±0.06	188±1.16	91.3±0.06	11.5±0.1	11.4

[a]The hydrogel naming (PwX_{SHz}-Y_{NBz}) denotes the structure of the hydrogel. With W = polymer content (wt%), X = number of arms of PEO-thiol macromer, Y = number of arms of PEO-norbornene macromer, and Z = molecular weight of the PEO precursor. [b]Calculated from the Flory-Rehner equation or the adapted form for ideal networks by neglecting chain ends.

the polymer fraction where the contribution of one of these two factors is maximal for the minimal of the other factor. This optimum can then be used to control the swelling behavior of the hydrogel. Returning to the enhanced swelling of the 10k rather than their 20k counterpart, there might be another explanation. For our system, the crosslinking efficiency is determined by the availability of the thiol and norbornene functional groups [50]. Increasing the molecular weight of the PEO norbornene crosslinker decreases the concentration of the functional end-group relative to the polymer concentration. Therefore, the probability for a thiol to be near a norbornene decreases, decreasing the crosslinking efficiency and leading to more network defects. Moreover, high molecular weight crosslinkers are prone to folding due to entanglements and intramolecular interactions, providing an additional hindrance for end-group encounters.

Water absorption into the polymeric network is affected by the elastically effective degree of crosslinking, which considers all chain segments that react elastically to elongation caused by swelling, therefore excluding those that form loops or have dangling chain ends. Thus, an ideal polymeric network consists only of elastically active chains. For clarity, elastically effective crosslinks can be either chemical, formed by a covalent bond, or physical, such as chain entanglements or strong intermolecular interactions [51, 52]. Our findings indicate that as the number of arms of the PEO building blocks (3SH-2NB < 4SH-2NB < 4SH-4NB) increases, the experimental swelling ratio ($Q_{m\ eq,\ actual}$) approaches those of an ideal network ($Q_{m\ eq,\ ideal}$) (S8). One might argue this is the result of increased crosslinking density.

Nevertheless, looking at the crosslinking densities for the gels made with 3_{SH1k} and 4_{SH2k} crosslinkers, we see that for the same polymer content and linear crosslinker, they differ within a range of only 20 mM. In contrast, for the same formulations, the differential increase of mass resulting from swelling was as high as 20%. Therefore, we can assume the difference in swelling behavior is due to an altered network structure rather than crosslinking density. Literature elucidated the following phenomenon; increasing the building blocks' functionality increases the network ideality. They argue the following, the number of elastically active chains (n_a) equals the number of functionalities (f_a) divided by two with $n_a > 1$, and $f_a > 2$ (linear chain) [46, 51]. Therefore, for each intramolecular loop, two functionalities will be sacrificed, decreasing the number of elastically active chains by one. Metters et al., 2005 showed that eight-arm PEO acrylate and linear PEO-thiol gels (> 40 wt%) matched the ideal swelling predictions, independent of the molecular weight of the precursors. In contrast, gels (> 40 wt%) made with low functionality precursors, four-arm PEO acrylate, and linear PEO thiol did not. So, more defects are formed at a lower degree of functionality and result in increased swelling ratios and water content. Network defects also impair the transparency of the hydrogels (S6).

Since in this work the number of functionalities equals the number of arms of the crosslinker, swelling caused by these elastically inactive loops or dead chain ends will be more apparent for crosslinkers with fewer arms [46]. For example, a loop on a three-armed molecule sacrifices two arms resulting in a dead chain end. For a four-arm, this would just result in the propagation of a linear chain. Even though norbornene functionalized chains will not homopolymerize, the formation of dithiols is possible. Therefore, this effect cannot be ignored. In summary, our data support the claim that augmenting the arm count leads to a hydrogel with improved ideal properties, resulting in reduced swelling.

For these hydrogels to be used in regenerative medicine, we must consider the following. Articular cartilage (AC) is 80% composed of water. Now, knowing that all hydrogels presented in this work swell until they reach an EWC between 91-98%, implantation into confined compartments, such as joints, leads to volume expansion, possibly interfering with cellular processes. Nevertheless, out of all the formulations, $P_{25}4_{SH2k}$-4_{NB20k} would be considered the best for cartilage regenerative applications as its EWC (91.3%) best approximates the water content of AC. For the hydrogels to reach an ECW of 80% for AC, a $Q_{m,\ eq\ ideal}$ of 5 is needed. The theoretical Flory-Rhener equation can be used to calculate the required Mc to achieve this desired ECW (S4). However, in general, we can say that a lower Q_m can be reached by decreasing the Mc, either by decreasing the molecular weight of the building blocks or increasing their functionality. Aside from altering the network structure, other methods to decrease swelling exist. In literature, several strategies to reduce hydrogel swelling have been suggested [21]. O'Shea et al., 2015 fabricated a non-swelling ethoxylated polyol thiol-ene-based hydrogel by integrating a hydrophobic ester bond into the precursor molecules and linking them to form a highly crosslinking network structure [53]. Aside from minimal swelling, scaffolds must have an appropriate pore size to facilitate cellular activities such as cell proliferation, cell growth, migration, nutrient supply, etc. For biomedical applications, literature advises micro-porous systems with a 10-100 nm mesh size. However, for cartilage application in specific, pore sizes of 100-500 µm are recommended for chondrocyte and mesenchymal stem cell proliferation. Meanwhile, the mesh size of the hydrogels presented in this work ranges between 10 and 22 nm and are therefore not ideal for cartilage regenerative medicine as they would impede cell infiltration proliferation and chondrogenesis [6, 54]. To limit swelling but also improve the biocompatibility for cellular processes, one could consider decreasing the overall crosslinking density but strive for a more ideal network by increasing the number of arms on the building block and/or incorporating anti-swelling strategies.

Mechanical testing

Aside from swelling, network architecture and hydrogel composition also affect the mechanical properties of hydrogels. In this section, a mechanical evaluation of the hydrogels discussed in the swelling section was performed by uniaxial compression testing. From this, the maximum stresses, E-moduli and toughness were calculated (S7).

Three-arm PEO hydrogels – Three-arm (1k) PEO thiol macromers were crosslinked to 6k, 10k, and 20k linear PEO norbornene to form PEO hydrogels with a polymer content of 20 and 25 wt%. The uniaxial compressive experimental results show that the as-prepared PEO hydrogels are extremely strong and tough (Figure 3). The maximum average stresses and E-moduli ranged between 3.3-4.4 MPa, and 108-178 kPa, respectively. The toughness of all gels, except 6k, was approximately 33 MJ/m3. All three-arm hydrogels, except for the 6k gel, can be compressed to 90% without fracturing (Figure 3a). The 6k gel was more brittle and cracked at a deformation of about 80% but could be further compressed until 90%. The fracture toughness was 26±3 MJ/m^3 and the toughness 48±4 MJ/m^3. The compression data

shows a general trend; increasing the molecular weight of the linear PEO norbornene crosslinker results in a decrease in mechanical strength. For example, the 6k 20 wt% gels could reach a maximum stress and E-modulus of 4.4±0.2 MPa, and 178±21 kPa, respectively. Whereas the 20k 25 wt% gels have the lowest, 3.4±0.1 MPa, and 108±3 kPa, respectively.

The compression results of the 10k gels show that with increasing polymer content from 20 wt% to 25 wt%, the compressive strength also increases. Although the difference is minimal, the E-moduli increase from 127±2.11 kPa for 20 wt% to 144±9.18 kPa for 25 wt% (Figure 3b). However, the compression findings for the 20k gels show a different trend. Specifically, the gels with 25 wt% polymer content had an E-modulus of 108±2.59 kPa, while those with 20 wt% exhibited an E-modulus of 121±4.85 kPa. Although these results initially appear to contradict expectations, the section on swelling analysis (above) demonstrates that the experimental crosslinking density for the 20k 25 wt% gels is also lower than that of their 20 wt% counterparts. Therefore, the swelling and compression test data support each other and confirm the direct relation between crosslinking density and mechanical strength.

Four-arm PEO thiol hydrogels – Four-arm (2k) PEO thiol macromers were crosslinked to linear (6k, 10k, and 20k) and four-arm (20k) PEO norbornene to form hydrogels with a polymer content of 20 and 25 wt%. Similar to the three-arm gels, the four-arm gels were found to be strong and tough (Figure 4). Here, the average maximum stresses and E-moduli ranged respectively between 4.3-16.4 MPa and 207-895 kPa, whereas the toughness ranged between 50-190 MJ/m^3. All four-arm hydrogels could be compressed to 90% without fracturing. Figures 4a and 4b show that maximum stress and E-moduli increase with increasing crosslinking density. The $P_{20}4_{SH2k}$-2_{NB10k} and $P_{20}4_{SH2k}$-2_{NB20k} show no clear differences in their maximum stresses, 4.3±0.1 MPa, and 4.6±0.2 MPa respectively. Increasing both the polymer concentration (Figures 4c and 4d) and the number of functionalities of the macromer building blocks (Figures 4e and 4f) results in stronger gels. Gels made with 4SH-4NB, 25 wt% reached an E-modulus of 895±10 kPa and a maximum stress of 16.4±0.6 MPa.

In tissue regeneration, scaffolds should offer structural support to surrounding tissues by providing a framework for cells to attach to and grow [5]. The hydrogels must be designed so their mechanical properties match those of the target tissue. If it is unable to bear these site-specific forces, the scaffold will disintegrate and fails to perform its intended function. By tuning the network topology and hydrogel composition, the mechanical properties of the scaffolds can be matched to those of specific tissues such as articular cartilage.

Hydrogel crosslinking density influences, aside from swelling behavior, the mechanical strength of hydrogels [55, 56]. Crosslinks form physical connections between polymer chains and provide resistance to mechanical forces by dissipating the energy throughout the network. This prevents localized rupture of the gel,

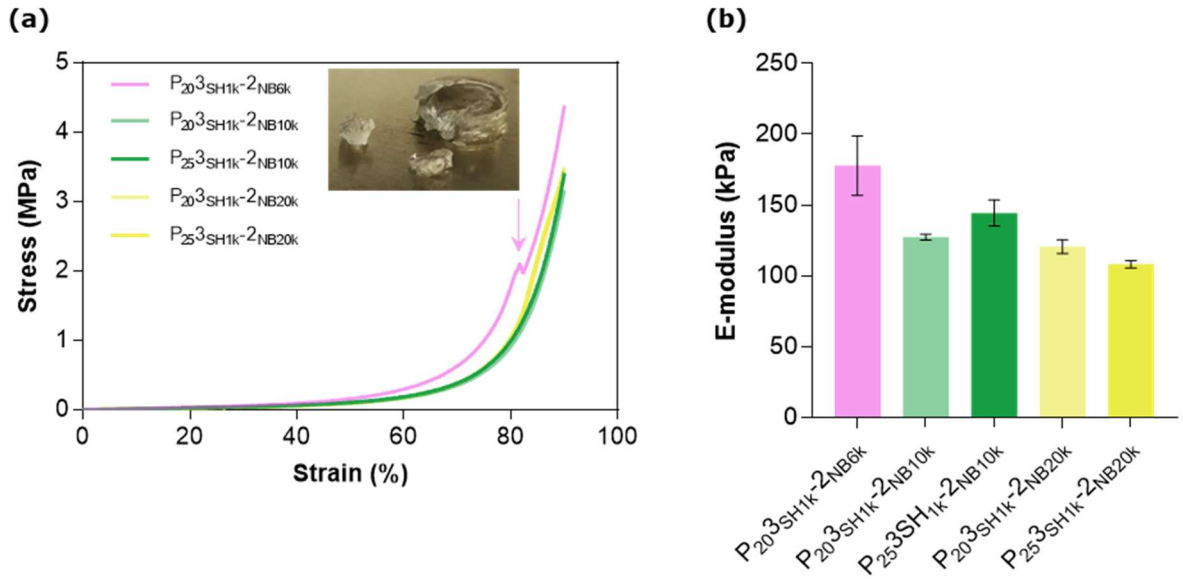

Figure 3: Mechanical evaluation of three-arm – linear PEO hydrogels. Hydrogels with three-arm (1k) PEO thiol and different molecular weights linear (6k, 10k, and 20k) PEO norbornene, 20 and 25 wt% polymer, were compression tested at a compress rate of 1 mm/s. The effect of increasing the molecular weight of the linear crosslinker and increasing the polymer content on the compressive robustness is shown. (a) Stress-strain curve of three-arm PEO thiol and linear PEO norbornene hydrogels (n=3) (b) E-moduli of three-arm PEO thiol – linear PEO norbornene (n=3). PEO, polyethene glycol; k, 10 0000; SH, thiol; NB, norbornene

resulting in improved toughness and strength. Nevertheless, it is not only the concentration of crosslinks but also the type of crosslinks (chemical or physical) that influences the material properties [57]. Chemical or covalent crosslinks are fixed, preventing chain mobility and resulting in a rigid and brittle gel. In contrast, physical crosslinks, such as entanglements or strong intermolecular interactions, are mobile and enhance energy dissipation. Therefore, hydrogels made with a high covalent-to-physical crosslink ratio exhibit low fracture energies [57]. In our work, the 6k gel had the highest covalent-to-physical crosslink ratio, as the length of the linear crosslinker limits the formation of chain entanglements. Consequently, the gels fractured at lower deformation, shown in figures 3a and 4a. In figure 4a, this fracture point seems more like an irregularity (arrow) in the trend. Nevertheless, there is a possibility that this point could become more discernible by increasing the sensitivity of the measurement. Next, increasing the polymer density, increases the load-carrying capacity of the material. This is because the fracture strength and stiffness of a polymer network are directly proportional to the number of polymer chains present per unit volume [58].

Besides crosslinking density and polymer content, the concentration of the photoinitiator (PI) used to crosslink the gels in the hydrogel affects the mechanical properties. Upon UV exposure, the PI forms radicals to initiate crosslinking. Therefore, increasing the amount of PI results in more reactive groups, increasing the crosslinking density of the network [59]. This effect was confirmed by varying the LAP concentration between 0.5 and 0.05 wt% for $P_{20}4_{SH2k}$-2_{NB10k} (S9). Therefore, it is important to point out that the three-arm gels were made with 0.3 wt% LAP, whereas 0.05 wt% for the four-arm. The difference in maximum stress and E-modulus between 0.3 wt% and 0.05 wt% were approximately 4 MPa and 150 kPa, respectively. Considering the genotoxic potential associated with the production of free radicals, it is advisable to limit the use of PI in bio-applications [60]. Nevertheless, the softness of the three-arm thiol gels posed a limitation, preventing the use of LAP concentrations below 0.3 wt%.

In figures 4e and 4f, the positive effect of macromer branching on the maximum stress and E-modulus is shown. Especially the gels made with 4_{SH2k}-4_{NB20k} were strong reaching E-moduli of 895±10 kPa. Replacing the 4_{NB20k} by 2_{NB20k}, decreased the modulus with 687 kPa. One might attribute these results to large variations in crosslinking density, however, this is not the case (164±0.14 mM for 4_{SH2k}-4_{NB20k} and 128±0.17 mM for 4_{SH2k}-2_{NB20k}). Similar to the swelling, greater branching of the PEO building blocks serves to alleviate the influence of network defects, thereby promoting a more homogeneous polymer network. This increased homogeneity results in a higher abundance of elastically active chains, which effectively disperse and withstand mechanical loads. As a result, the mechanical robustness of the PEO hydrogel is improved [46]. Replacing the 4_{SH2k} by a 3_{SH1k}, the E-modulus decreases from 208±2 to 108±3 kPa. Also, here, this difference is most likely not due to decreased crosslinking density (128±0.17 mM for 4_{SH2}-2_{NB20} and 115±0.06 mM for 3_{SH1k}-2_{NB20k}). Not to mention that the difference in mechanical strength would be even more apparent if the 3SH and 4SH gels were made at identical LAP concentrations.

The gels presented in this work demonstrated superior performance compared to other examples of thiol-ene photo click multi-arm PEO hydrogels from the literature.

In a study by Mc Dougall et al., 2017, they investigated the swelling and mechanical properties of thiol-ene photoclick hydrogels made using three-arm PEO (1k) -or four-arm PEO (2k) alkyne and bifunctional PEO (1k, 2k, 4k) thiol [42]. In accordance with the results reported in this research, they observed that increasing the functionality of the building blocks increased their swelling and mechanical performance. They obtained the highest maximum stress for $P_{10}4_{A2k}$-2_{SH4k}, 72 kPa. Meanwhile, $P_{10}4_{A2k}$-2_{SH2k} had the highest E-modulus 72 kPa.

Fiedler et al., 2016 investigated the mechanical properties of eight-arm PEO norbornene (10k) and dithiol PEO (1k) hydrogels at different polymer concentrations (5, 10, 20 wt%) and thiol:ene ratios [48]. A 10 wt% hydrogel made with 0.05 wt% LAP and a 1:1 thiol:ene ratio showed a compressive modulus of ± 90 kPa. However, the research aimed to improve the mechanical performance of the hydrogels by first crosslinking in off-stochiometric ratios of thiol:ene (>1) and subsequently crosslinking the free norbornene ends by cyclic soaking the gels in a dithiol containing PBS solution. At their optimum, the 20 wt% PEO hydrogels showed a compressive modulus of ± 320 kPa, maximum stress of ± 440 kPa, and toughness ± 115 kJ/m^3.

Depending on the depth within the articular cartilage and the direction of the collagen fibers relative to that of the exerted mechanical force, the E-modulus of articular cartilage under unconfined compression ranges between 100-1600 kPa [61-64]. In this study, by manipulating only the network architecture of the PEO hydrogels, it was possible to achieve a controlled variation in the E-modulus within half of this range, specifically between 108-895 kPa. However, increasing the number of functionalities of the building blocks might

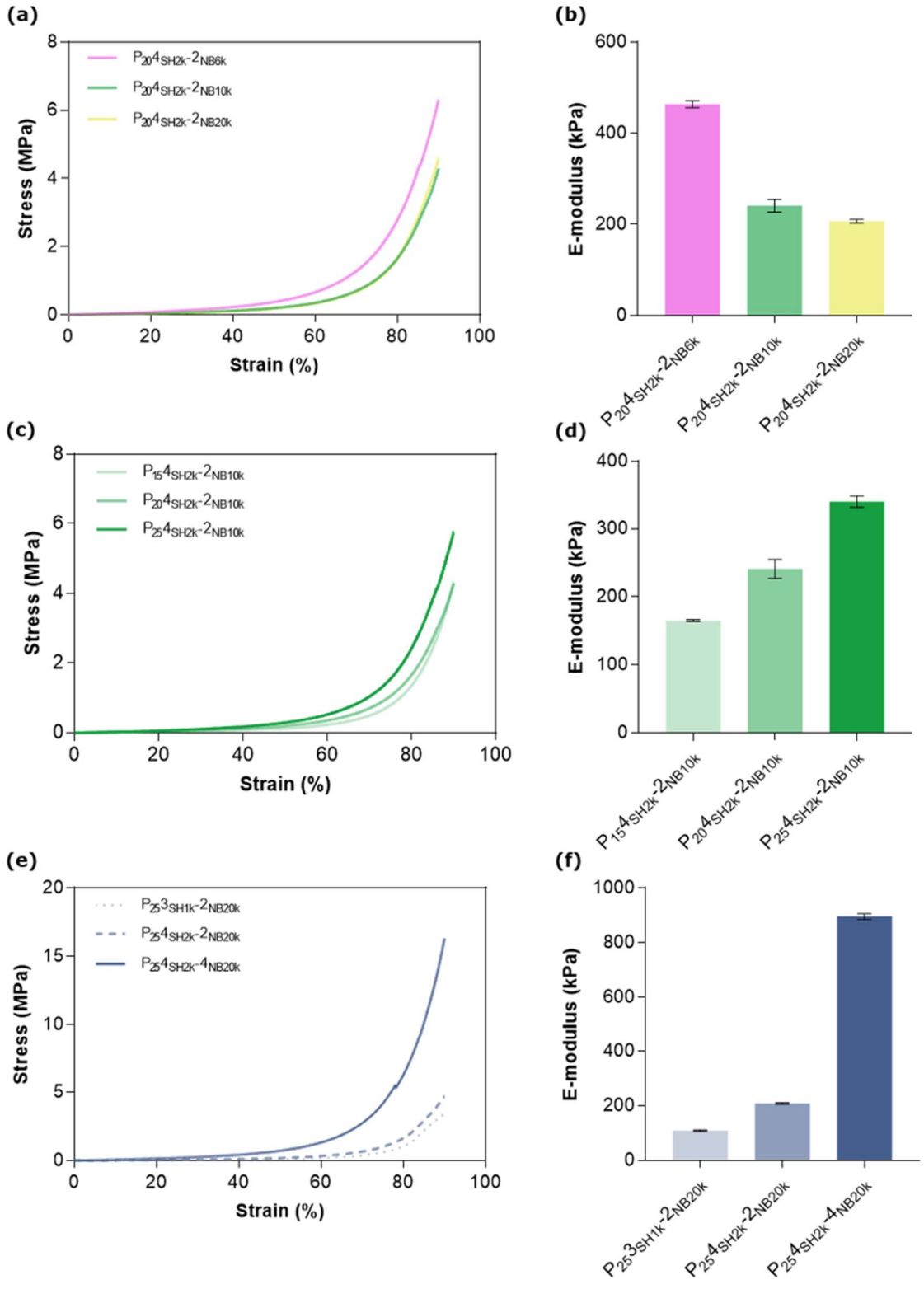

Figure 4: Mechanical evaluation of four-arm PEO thiol hydrogels. Hydrogels with four-arm (2k) PEO and either linear (6k, 10k, and 20k) or four-arm PEO norbornene were compression tested at a compress rate of 1 mm/s. Changing structural parameters on the maximum stress and E-moduli of the PEO hydrogels: (a,b) The effect of increasing the length of the linear crosslinker from 6k to 20k (n=4) (c,d) Effect of polymer concentration 15 wt% to 25 wt% (n=4) (e,f) Effect of branching of the PEO building blocks (n=3). PEO, polyethene glycol; k, 10 0000; SH, thiol; NB, norbornene

unlock part of the range that could not be reached.

Within the body, cartilage experiences repetitive loading. However, in our analysis, we only examined the mechanical properties of the hydrogels after a single compression cycle, leaving us unsure about their recovery behavior. To gain insight into their mechanical performance in vivo, it would be beneficial to conduct cyclic compression testing. This would allow us to observe how the hydrogels respond to repeated loading and better understand their behavior in a more realistic physiological setting. Earlier, it was established that the hydrogels utilized in this study will undergo swelling upon integration into the articular cartilage environment. Consequently, their mechanical properties will be altered and differ from the previously described results, leading us into the next section.

Swollen four-arm PEO norbornene (20k) hydrogel– The mechanical properties of hydrogels formed by crosslinking four-arm (2k) PEO thiol crosslinked to four-arm (20k) PEO norbornene at 25 wt%, were analyzed at different stages in the swelling (non-swollen, 24h and 48). Since the $P_{25}4_{SH2k}$-4_{NB20k} gels reached equilibrium after 30h, the 48h swelling will be referred to as equilibrium (Eq). The uniaxial compression results showed that swelling drastically decreases resistance to mechanical stress. In a non-swollen state, the hydrogels withstood maximum stresses of 16.4±0.6 MPa. After 24h of swelling, this value decreased to 0.45±0.15 MPa and 0.38±0.09 MPa at equilibrium. Swelling resulted in softer hydrogels, as the E-modulus decreased from 895±10 kPa, non-swollen, to 244±19 kPa at 24h and 359±61 at equilibrium. The toughness of the gels at 24h of swelling and equilibrium was similar, 7.5±2.3 MJ/m^3 and 7.0±1.7 MJ/m^3, respectively, whereas that of the non-swollen gel was 190±6 MJ/m^3.

Literature states that with increasing degrees of swelling, the stiff- and toughness of the hydrogels decrease [65]. In swollen state, the polymer chain of the hydrogels network is stretched. So, when external stress is applied, the chains are unable to expand further. Additionally, physical crosslinks are loosened as water enters the network, lowering the crosslinking density and impairing energy dissipation throughout the network. Because of this, swollen hydrogels break at lower strains (S10) [57]. Relative to the hydrogel's end volume, increasing the water content results in a decreased polymer concentration, expecting a decrease in mechanical performance. However, against expectations, the compression results reveal that the equilibrium swollen hydrogel is stiffer compared to the 24h swollen one. A possible explanation might be that at low deformations (like the region where the E-modulus is determined), the polymer chains of the equilibrium swollen gels are more elongated and, therefore, less stretchable than their less swollen version which expresses itself with a higher E-modulus. If more stress is applied, additional chain elongation is prevented, resulting in premature fracturing, decreasing the fracturing stress and strain as seen in the compression results (S10). The toughness of hydrogels is directly related to polymer density, hence decreasing with increasing degrees of swelling [65]. However, other factors, such as swelling-caused degradation or diffusion of uncrosslinked material, could influence the mechanical performance of the hydrogels. Lin et al., 2021 investigated the degradation of a 2.5 wt% PEO hydrogel made with eight-arm PEO norbornene and linear PEO thiol based on the stability of the mass swelling ratio (Q_m). They showed that even after 8 days of swelling in PBS at 37°C, the Q_m remained constant (30), indicating that the gel did not degrade [66]. Hunckler et al., 2019 found even more

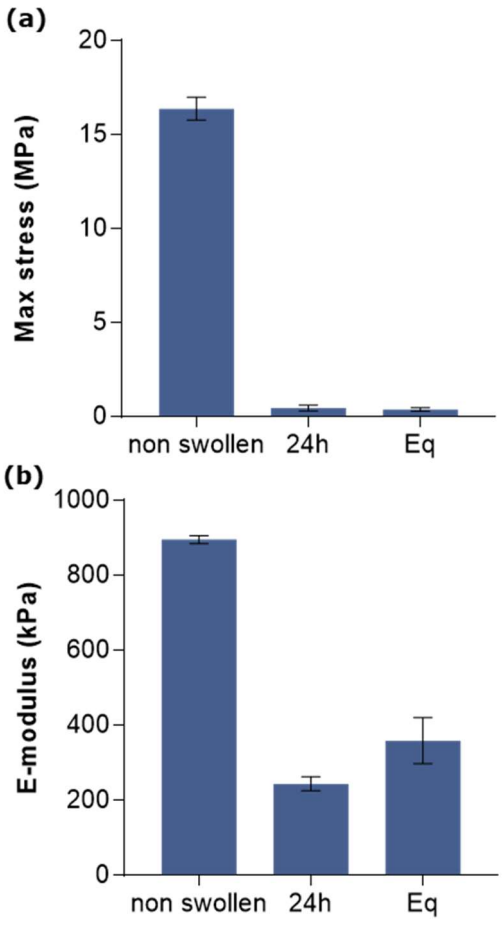

Figure 5: The effect of swelling on the mechanical properties of PEO hydrogels. Four-arm PEO (2k) thiol and four-arm PEO (20k) norbornene 25 wt% hydrogels were compression tested at 1 mm/s at different stages in swelling: non-swollen, 24h swelling and equilibrium. (a) Maximum stress (n=3) (b) E-modulus (n=3). h, hour; Eq, equilibrium.

impressive results. Here, a 5 wt% thiol-ene four-arm (20k) and dithiol PEO gels showed no signs of degradation after 68 days of swelling in PBS [67]. Furthermore, the degradation of thiol-ene gels is found to be pH dependent. A study showed that a four-arm PEO-norbornene linear PEO thiol gel swollen in PBS at pH 6 had a constant Q_m over a 45-day period. For the same gel, increasing the pH to 8, resulted in faster degradation (18 days) [40]. Because the synthesis of PEO norbornene and thiol takes place in an acidic environment, the pH of the gels was slightly acidic (pH 6). Also, hydrogels with low polymer concentrations are found to have higher degradation rates. With this information, it is safe to assume that the decrease seen in mechanical strength is likely not the result of degradation.

The swelling of hydrogels facilitates the extraction of uncrosslinked material and free molecules, such as PI, out of the hydrogel. Glover et al., 2020 showed that the removal of free molecules and unreacted material out of Sylgard 184, a commercially available PDMS elastomer, results in higher toughness, E-modulus, and stretchability. Another study showed that the presence LAP does not influence swelling or mechanical properties [48]. By removal of this excess material, the volume of the hydrogel decreases, increasing the polymer concentration per volume unit and the strength of the material [68]. This again shows the importance of network ideality, where a 100% reaction efficiency is expected, leaving no unreacted material behind.

Unexpectedly, the degradation of these hydrogels in vitro and in vivo differs significantly. Hunckler et al., 2019 investigated the degradation behavior of four-arm PEO norbornene (20k) and linear PEO thiol (5k) hydrogels, 5 wt% when implanted into the intraperitoneal space of rodents. They showed that after 24h, the gels were completely degraded. However, for the same hydrogel composition but with a less hydrolytically sensitive amide linkage connecting the functional groups to the PEO, the degradation was delayed up to 68 days after implantation. Additionally, they showed that changing the ester bond to an amine bond only influenced the gelation time, still within reasonable range (< 10s), at low concentration of LAP (0.02 wt%) [67]. In the future, one might consider switching out the ester-bond for a m ore degradation-resistant bonding type to alter the degradation of thiol-norbornene PEO hydrogels.

From the mechanical characterization of hydrogels with different network structures, it can be concluded that the mechanical properties could be tuned by varying the crosslinking density and degree of functionality [69]. Furthermore, it was found that swelling decreases the mechanical performance of the hydrogels.

DLP printing

Next, the printability and gelation time of 20 wt% and 25 wt% 4_{SH2k}-$2_{NB6,10,20k}$ was investigated by performing a one-layer experiment using a 405 nm DLP printer (Figure 6). In this experiment, an image of a square was projected eight times onto the pre-hydrogel resin for varying time intervals, for each square decreasing from 9s to 2s, with increments of 1s. Black indicates what should be crosslinked, whereas the white region should not be crosslinked.

The results showed that for all formulations, the projected image gelated after only 2s exposure to UV light (figure 6b). With increasing exposure time, the resolution of the printed image decreased seen by the

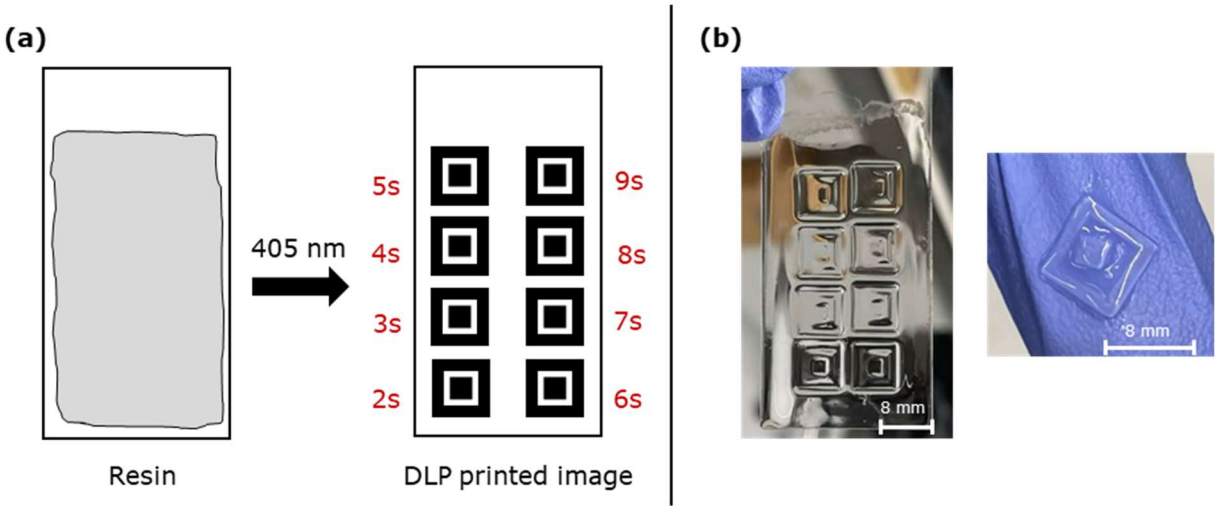

Figure 6: One-layer DLP printing experiment using four-arm PEO (2k) thiol and linear PEO (6k, 10k, and 20k) norbornene resin and varying 405 nm exposure time (2-9s) (a) schematic representation of experimental procedure (b) picture of DLP printed $P_{20}4_{SH2k}$-2_{NB10k} resin. In this experiment, constant LAP concentrations of 0.5 wt% were maintained; scale bar 8 mm

attachment of the small squares to the outer square structure.

For 3D printing purposes, fast gelation enables the maintenance of the shape integrity of the printed structure. The gelation time depends on the speed of the crosslinking reactions, thus the reactivity of the reactive groups and the concentration of the PI.
The thiol—norbornene photo click reaction proceeds via a radical-mediated step-growth polymerization mechanism [70]. The crosslinking reaction is initiated by the UV-mediated decomposition of the PI into radicals. The radical abstracts a hydrogen from the thiol end group, forming a thiyl radical that reacts with the strained ene-bond in the norbornene moiety attached to PEO, forming a thioether bond and a carbon-centered radical. This radical can react again with another thiol, repeating the same mechanism. This sequence of thiyl formation and norbornene coupling proceeds in stochiometric ratio until one of the reactive groups (either thiol or norbornene) is depleted. The speed of the crosslinking reaction is the result of high reactivity between the thiol and norbornene. Because of this, the presence of oxygen does not inhibit this reaction, further enhancing its efficiency. No homopolymerization between norbornene groups is possible; hence the polymerized network only has bio-orthogonal crosslinks. An additional advantage of thiol-ene reactions is that they can take place under mind conditions and low concentrations of PI, making thiol-ene reactions ideal for bio-applications such as tissue engineering [70].

It must be pointed out that the resin used for printing contained 0.5 wt% LAP. However, minimally required concentrations of LAP that still allow gelation within a decent time frame are preferred. To gauge the effect of decreasing the LAP on the gelation time, an identical experiment was performed on one type of resin, $P_{25}4_{SH2k}$-2_{NB10k}, at 0.05 wt% LAP. Also, here the gelation occurred within 2s (S11). Nevertheless, literature shows that rheology-based determination of the gelation time is much lower than this. For example, Holmes et al., 2017 showed that a 3.5 wt% collagen-PEG hydrogels with 0.2 wt% LAP gelled after 0.03s of exposure to 365 nm UV light [60]. Research by Kim et al., 2023 showed that a 5 wt% gel made from PEO-8NB (20k) and PEO-4SH, 0.3 wt% LAP subjected to 405 nm light gelled in less than 1s and cured in 3s [35]. Also, it was seen that increasing the polymer concentration resulted in delayed gelation times. In contrast to the aforementioned, the resin formulation in this work had a higher polymer density (20 wt%). Although a rheology curing time sweep would provide more detailed information, it can be assumed that the gelation point for our gels lays between 1 and 2s. Changing the UV light from 405 nm to 365 nm, closer to the maximal absorbance range of LAP, would enhance the radical formation hence the gelation efficiency.

Of course, in this experiment, only one layer was printed. As previously established, increasing UV exposure time decreases the resolution of the printed structure by unwanted crosslinking due to background light of the laser. Thus, when printing 3D instead of 2D structures, the processing time and UV exposure time increase, leading to photocrosslinking in unwanted areas. To circumvent this, one can make use of filters that are placed over the light source or photo absorbers, like tartrazine, that are added to the resin. Tartrazine is a yellow color pigment that has a maximum absorbance at 460 nm, best approaching the wavelength of the DLP projector light to absorb the light noise [71]. Even though both delay the gelation time (6s for 0.08 wt% tartrazine), there still seems to be a manageable time frame in which the resin could gelate. Concentrations of tartrazine of 1.1 wt% and up prevented thiol-norbornene gelation completely [35].

Aside from this, the optimization of light exposure is an important aspect of the DLP printing procedure. In DLP printing, 3D structures are printed in Z-stacks. By over-exposure to UV light, the light penetrates out of the focal plane resulting in over-crosslinking, and losing the desired shape [72]. In a study by Seo et al., 2022 where they 3D printed PEODMA hydrogels, they set the layer thickness of 100 µm. However, they saw that at low UV exposures, the light could not penetrate, whereas over-exposure resulted in over-crosslinking [72].

CONCLUSION

This study aimed to fabricate mechanically robust thiol-norbornene photo-click poly(ethene oxide) (PEO) hydrogels with favorable swelling behavior for articular cartilage tissue regeneration applications. Instead of relying on complex toughening strategies, we achieved this by enhancing intrinsic strength through the alteration of the network topology. Varying molecular weights of linear and multi-arm functionalized PEO were crosslinked to create hydrogels with different network architectures. The mechanical and swelling analysis revealed that the network architecture, rather than the crosslinking density, significantly influenced the performance of the PEO hydrogels. Increased branching of the PEO building blocks resulted in a more uniform network with minimal defects, approaching an "ideal network" and explaining the improved mechanical and swelling behavior. While our study partially met the mechanical requirements for hydrogels in articular cartilage regeneration and outperformed similar multi-arm PEO hydrogels, there is still room for improvement. The porosity of the PEO hydrogels produced in this study was insufficient for biomedical and cartilage applications.

Nonetheless, our findings inspire further exploration of combined PEO building block options, variations in the number of branches in PEO precursors, and varying polymer densities.

In addition to the mechanical aspects, we verified the printability and rapid gelation (2s) of the hydrogels presented in this research. Although no 3D constructs were printed in this study, it underscores the potential of these photocurable 3D bio-printed hydrogel scaffolds. Overall, our study provides valuable insights for the development of mechanically robust and printable hydrogels, motivating further investigations into optimizing various parameters for the fabrication of bio-printed hydrogel scaffolds.

REFERENCES

1. Sophia Fox AJ, Bedi A Fau - Rodeo SA, Rodeo SA. The basic science of articular cartilage: structure, composition, and function. (1941-7381 (Print)).
2. Iwamoto M, Ohta Y Fau - Larmour C, Larmour C Fau - Enomoto-Iwamoto M, Enomoto-Iwamoto M. Toward regeneration of articular cartilage. (1542-9768 (Electronic)).
3. Das SK, Farooqi A. Osteoarthritis. (1521-6942 (Print)).
4. Liu Y, Shah KM, Luo J. Strategies for Articular Cartilage Repair and Regeneration. (2296-4185 (Print)).
5. El-Sherbiny IM, Yacoub MH. Hydrogel scaffolds for tissue engineering: Progress and challenges. (2305-7823 (Print)).
6. Zhou L, Guo P, D'Este M, Tong W, Xu J, Yao H, et al. Functionalized Hydrogels for Articular Cartilage Tissue Engineering. Engineering. 2022;13:71-90.
7. Cheng A, Schwartz Z, Kahn A, Li X, Shao Z, Sun M, et al. Advances in Porous Scaffold Design for Bone and Cartilage Tissue Engineering and Regeneration. (1937-3376 (Electronic)).
8. Spicer CD. Hydrogel scaffolds for tissue engineering: the importance of polymer choice. Polymer Chemistry. 2020;11(2):184-219.
9. Ning X, Huang J, A Y, Yuan N, Chen C, Lin D. Research Advances in Mechanical Properties and Applications of Dual Network Hydrogels. International Journal of Molecular Sciences [Internet]. 2022; 23(24).
10. Katsuno C, Konda A Fau - Urayama K, Urayama K Fau - Takigawa T, Takigawa T Fau - Kidowaki M, Kidowaki M Fau - Ito K, Ito K. Pressure-responsive polymer membranes of slide-ring gels with movable crosslinks. (1521-4095 (Electronic)).
11. Imran AB, Seki T, Takeoka Y. Recent advances in hydrogels in terms of fast stimuli responsiveness and superior mechanical performance. Polymer Journal. 2010;42(11):839-51.
12. Xin H. Double-Network Tough Hydrogels: A Brief Review on Achievements and Challenges. LID - 10.3390/gels8040247 [doi] LID - 247. (2310-2861 (Electronic)).
13. Xu X, Jerca FA, Van Hecke K, Jerca VV, Hoogenboom R. High compression strength single network hydrogels with pillar[5]arene junction points. Materials Horizons. 2020;7(2):566-73.
14. Huang S, Hong X, Zhao M, Liu N, Liu H, Zhao J, et al. Nanocomposite hydrogels for biomedical applications. Bioengineering & Translational Medicine. 2022;7(3):e10315.
15. Zhang XN, Zheng Q, Wu ZL. Recent advances in 3D printing of tough hydrogels: A review. Composites Part B: Engineering. 2022;238:109895.
16. Bashir SA-O, Hina MA-O, Iqbal J, Rajpar AH, Mujtaba MA-O, Alghamdi NA, et al. Fundamental Concepts of Hydrogels: Synthesis, Properties, and Their Applications. LID - 10.3390/polym12112702 [doi] LID - 2702. (2073-4360 (Electronic)).
17. Zhu J. Bioactive modification of poly(ethylene glycol) hydrogels for tissue engineering. (1878-5905 (Electronic)).
18. Drury JL, Mooney DJ. Hydrogels for tissue engineering: scaffold design variables and applications. Biomaterials. 2003;24(24):4337-51.
19. Liu SQ, Tay R, Khan M, Rachel Ee PL, Hedrick JL, Yang YY. Synthetic hydrogels for controlled stem cell differentiation. Soft Matter. 2010;6(1):67-81.
20. Bian S, Hao L, Qiu X, Wu J, Chang H, Kuang G-M, et al. An Injectable Rapid-Adhesion and Anti-Swelling Adhesive Hydrogel for Hemostasis and Wound Sealing. Advanced Functional Materials. 2022;32(46):2207741.
21. Zhan Y, Fu W, Xing Y, Ma X, Chen C. Advances in versatile anti-swelling polymer hydrogels. Materials Science and Engineering: C. 2021;127:112208.
22. Wu F, Pang Y, Liu J. Swelling-strengthening hydrogels by embedding with deformable nanobarriers. Nature Communications. 2020;11(1):4502.
23. Peppas NA, Keys KB, Torres-Lugo M, Lowman AM. Poly (ethylene glycol)-containing hydrogels in drug delivery. Journal of controlled release. 1999;62(1-2):81-7.
24. Bashir S, Hina M, Iqbal J, Rajpar AH, Mujtaba MA, Alghamdi NA, et al. Fundamental Concepts of Hydrogels: Synthesis, Properties, and Their Applications. Polymers [Internet]. 2020; 12(11).
25. Lin C-C, Raza A, Shih H. PEG hydrogels formed by thiol-ene photo-click chemistry and their effect on the formation and recovery of insulin-secreting cell spheroids. Biomaterials. 2011;32:9685-95.
26. Laurano R, Boffito M, Cassino C, Midei L, Pappalardo R, Chiono V, et al. Thiol-Ene Photo-Click Hydrogels with Tunable Mechanical Properties Resulting from the Exposure of

Different -Ene Moieties through a Green Chemistry. Materials [Internet]. 2023; 16(5).
27. Ravarino P, Panja S, Adams DJ. Spatiotemporal Control Over Base-Catalyzed Hydrogelation Using a Bilayer System. Macromolecular Rapid Communications. 2022;43(23):2200606.
28. Nguyen KT, West JL. Photopolymerizable hydrogels for tissue engineering applications. Biomaterials. 2002;23(22):4307-14.
29. Van Hoorick J, Dobos A, Markovic M, Gheysens T, Van Damme L, Gruber P, et al. Thiol-norbornene gelatin hydrogels: influence of thiolated crosslinker on network properties and high definition 3D printing. Biofabrication. 2021;13(1):015017.
30. Lin CC, Ki CS, Shih H. Thiol-norbornene photo-click hydrogels for tissue engineering applications. LID - 41563 [pii]. (0021-8995 (Print)).
31. Gao Q, Kim B-S, Gao G. Advanced Strategies for 3D Bioprinting of Tissue and Organ Analogs Using Alginate Hydrogel Bioinks. Marine Drugs [Internet]. 2021; 19(12).
32. Advincula RC, Dizon JRC, Caldona EB, Viers RA, Siacor FDC, Maalihan RD, et al. On the progress of 3D-printed hydrogels for tissue engineering. MRS Communications. 2021;11(5):539-53.
33. Taneja H, Salodkar SM, Singh Parmar A, Chaudhary S. Hydrogel based 3D printing: Bio ink for tissue engineering. Journal of Molecular Liquids. 2022;367:120390.
34. Ding H, Dong M, Zheng Q, Wu ZL. Digital light processing 3D printing of hydrogels: a minireview. Molecular Systems Design & Engineering. 2022;7(9):1017-29.
35. Kim MH, Lin C-C. Poly(ethylene glycol)–Norbornene as a Photoclick Bioink for Digital Light Processing 3D Bioprinting. ACS Applied Materials & Interfaces. 2023;15(2):2737-46.
36. Leonards H, Engelhardt S, Hoffmann A, Pongratz L, Schriever S, Bläsius J, et al. Advantages and drawbacks of Thiol-ene based resins for 3D-printing2015. 93530F p.
37. Baier Leach J, Bivens Ka Fau - Patrick CW, Jr., Patrick Cw Jr Fau - Schmidt CE, Schmidt CE. Photocrosslinked hyaluronic acid hydrogels: natural, biodegradable tissue engineering scaffolds. (0006-3592 (Print)).
38. Zustiak SP, Leach JB. Hydrolytically degradable poly(ethylene glycol) hydrogel scaffolds with tunable degradation and mechanical properties. (1526-4602 (Electronic)).
39. Kędzierska M, Bańkosz M, Potemski P. Studies on the Impact of the Photoinitiator Amount Used during the PVP-Based Hydrogels’ Synthesis on Their Physicochemical Properties. Materials [Internet]. 2022; 15(17).
40. Shih H, Lin CC. Crosslinking and degradation of step-growth hydrogels formed by thiol-ene photoclick chemistry. Biomacromolecules. 2012;13(7):2003-12.
41. Flory PJ, Rehner J, Jr. Statistical Mechanics of Crosslinked Polymer Networks II. Swelling. The Journal of Chemical Physics. 2004;11(11):521-6.
42. Macdougall LJ, Truong VX, Dove AP. Efficient In Situ Nucleophilic Thiol-yne Click Chemistry for the Synthesis of Strong Hydrogel Materials with Tunable Properties. ACS Macro Letters. 2017;6(2):93-7.
43. Yang X, Dargaville BL, Hutmacher DW. Elucidating the Molecular Mechanisms for the Interaction of Water with Polyethylene Glycol-Based Hydrogels: Influence of Ionic Strength and Gel Network Structure. Polymers (Basel). 2021;13(6).
44. Hoti G, Caldera F, Cecone C, Rubin Pedrazzo A, Anceschi A, Appleton SL, et al. Effect of the Crosslinking Density on the Swelling and Rheological Behavior of Ester-Bridged β-Cyclodextrin Nanosponges. Materials (Basel). 2021;14(3).
45. Nguyen QT, Hwang Y, Chen AC, Varghese S, Sah RL. Cartilage-like mechanical properties of poly (ethylene glycol)-diacrylate hydrogels. Biomaterials. 2012;33(28):6682-90.
46. Metters A, Hubbell J. Network Formation and Degradation Behavior of Hydrogels Formed by Michael-Type Addition Reactions. Biomacromolecules. 2005;6(1):290-301.
47. Toepke MW, Impellitteri NA, Theisen JM, Murphy WL. Characterization of Thiol-Ene Crosslinked PEG Hydrogels. Macromolecular Materials and Engineering. 2013;298(6):699-703.
48. Fiedler CI, Aisenbrey EA, Wahlquist JA, Heveran CM, Ferguson VL, Bryant SJ, et al. Enhanced mechanical properties of photo-clickable thiol–ene PEG hydrogels through repeated photopolymerization of in-swollen macromer. Soft Matter. 2016;12(44):9095-104.
49. Kong D-C, Yang M-H, Zhang X-S, Du Z-C, Fu Q, Gao X-Q, et al. Control of Polymer Properties by Entanglement: A Review. Macromolecular Materials and Engineering. 2021;306(12):2100536.
50. Michel SES, Rogers SE, Briscoe WA-OX, Galan MA-O. Tunable Thiol-Ene Photo-Cross-Linked Chitosan-Based Hydrogels for Biomedical Applications. (2576-6422 (Electronic)).
51. Lenzi F, Sannino A, Borriello A, Porro F, Capitani D, Mensitieri G. Probing the degree of crosslinking of a cellulose based superabsorbing hydrogel through traditional and NMR techniques. Polymer. 2003;44(5):1577-88.
52. Flory PJ, Erman B. Theory of elasticity of polymer networks. 3. Macromolecules. 1982;15(3):800-6.

53. O'Shea TM, Aimetti Aa Fau - Kim E, Kim E Fau - Yesilyurt V, Yesilyurt V Fau - Langer R, Langer R. Synthesis and characterization of a library of in-situ curing, nonswelling ethoxylated polyol thiol-ene hydrogels for tailorable macromolecule delivery. (1521-4095 (Electronic)).
54. Ganji F, Vasheghani Farahani S, Vasheghani-Farahani E. Theoretical Description of Hydrogel Swelling: A Review. Iranian Polymer Journal. 2010;19:375-98.
55. Martinez AW, Caves Jm Fau - Ravi S, Ravi S Fau - Li W, Li W Fau - Chaikof EL, Chaikof EL. Effects of crosslinking on the mechanical properties, drug release and cytocompatibility of protein polymers. (1878-7568 (Electronic)).
56. Shokuhfar A, Arab B. The effect of cross linking density on the mechanical properties and structure of the epoxy polymers: molecular dynamics simulation. Journal of Molecular Modeling. 2013;19(9):3719-31.
57. Norioka C, Inamoto Y, Hajime C, Kawamura A, Miyata T. A universal method to easily design tough and stretchable hydrogels. NPG Asia Materials. 2021;13(1):34.
58. Ji D, Kim J. Recent Strategies for Strengthening and Stiffening Tough Hydrogels. Advanced NanoBiomed Research. 2021;1(8):2100026.
59. Khandaker M, Orock A, Tarantini S, White J, Yasar O. Biomechanical Performances of Networked Polyethylene Glycol Diacrylate: Effect of Photoinitiator Concentration, Temperature, and Incubation Time. (1687-8787 (Print)).
60. Holmes R, Yang XA-O, Dunne A, Florea LA-O, Wood D, Tronci GA-O. Thiol-Ene Photo-Click Collagen-PEG Hydrogels: Impact of Water-Soluble Photoinitiators on Cell Viability, Gelation Kinetics and Rheological Properties. LID - 10.3390/polym9060226 [doi] LID - 226. (2073-4360 (Electronic)).
61. Lyyra-Laitinen T, Niinimäki M, Töyräs J, Lindgren R, Kiviranta I, Jurvelin JS. Optimization of the arthroscopic indentation instrument for the measurement of thin cartilage stiffness. Physics in Medicine & Biology. 1999;44(10):2511.
62. Korhonen R, Laasanen M, Töyräs J, Rieppo J, Hirvonen J, Helminen H, et al. Comparison of the equilibrium response of articular cartilage in unconfined compression, confined compression and indentation. Journal of biomechanics. 2002;35(7):903-9.
63. Jurvelin J, Buschmann M, Hunziker E. Optical and mechanical determination of Poisson's ratio of adult bovine humeral articular cartilage. Journal of biomechanics. 1997;30(3):235-41.
64. Silver FH, Bradica G, Tria A. Elastic energy storage in human articular cartilage: estimation of the elastic modulus for type II collagen and changes associated with osteoarthritis. Matrix Biology. 2002;21(2):129-37.
65. Kessler M, Yuan T, Kolinski JM, Amstad E. Influence of the Degree of Swelling on the Stiffness and Toughness of Microgel-Reinforced Hydrogels. Macromolecular Rapid Communications. 2023;n/a(n/a):2200864.
66. Lin F-Y, Lin C-C. Facile Synthesis of Rapidly Degrading PEG-Based Thiol-Norbornene Hydrogels. ACS Macro Letters. 2021;10(3):341-5.
67. Hunckler MA-O, Medina JD, Coronel MA-O, Weaver JA-O, Stabler CA-O, García AA-O. Linkage Groups within Thiol-Ene Photoclickable PEG Hydrogels Control In Vivo Stability. (2192-2659 (Electronic)).
68. Glover JD, McLaughlin CE, McFarland MK, Pham JT. Extracting uncrosslinked material from low modulus sylgard 184 and the effect on mechanical properties. Journal of Polymer Science. 2020;58(2):343-51.
69. Jiang Z, Shaha R, McBride R, Jiang K, Tang M, Xu B, et al. Crosslinker length dictates step-growth hydrogel network formation dynamics and allows rapid on-chip photoencapsulation. Biofabrication. 2020;12(3):035006.
70. Cramer NB, Bowman CN. Kinetics of thiol–ene and thiol–acrylate photopolymerizations with real-time fourier transform infrared. Journal of Polymer Science Part A: Polymer Chemistry. 2001;39(19):3311-9.
71. Okeola FO, Odebunmi EO, Amoloye MA, Babamale HF, Thema S, Abdulsalam JO. Kinetic and Thermodynamic Study of Oxidative Decolourisation of a Typical Food Dye (Tartrazine) in an Aqueous Environment. Journal of Applied Sciences en Environmental Management. 2020;24.
72. Seo JW, Kim GM, Choi Y, Cha JM, Bae H. Improving Printability of Digital-Light-Processing 3D Bioprinting via Photoabsorber Pigment Adjustment. International Journal of Molecular Sciences [Internet]. 2022; 23(10).

Acknowledgements – The author is grateful to M. Ebrahimi for guidance, supervision, feedback, and help with the interpretation of the results throughout the internship. Also, thanks to M. Campos for helping to perform the DLP printing experiments and sharing her knowledge on this subject. Furthermore, thanks to K. Van Vinckenroye for technical support, V. Atella for mental support and interchange of ideas, and all member of the AFP group for the pleasant working environment. A special thanks to S. Driesen who was always ready to help when needed. At last, the author would like to thank the group leader, L. Pitet, for arranging this internship, providing feedback and creating a positive group attitude.

Author contributions – L. Pitet and M. Ebrahimi developed the research design. U. Arickx and M. Ebrahimi performed the data collection and interpretated the results. Writing of the paper was done by U. Arickx. Collenction of H-NMR data was performed by K. Van Vinckenroye. All authors carefully read and edited the paper.

SUPPLEMENTARY

S1: Compositions of all hydrogels in this work. Hydrogels were formulated with [SH]:[NB] of 1:1.

Hydrogel[a]	PEG-SH	PEG-NB	Polymer (wt%)	LAP (wt%)
$P_{20}3_{SH1k}$-2_{NB6k}	3-arm, 1k	Linear, 6k	20	0.3
$P_{25}3_{SH1k}$-2_{NB6k}	3-arm, 1k	Linear, 6k	25	0.3
$P_{20}3_{SH1k}$-2_{NB10k}	3-arm, 1k	Linear, 10k	20	0.3
$P_{25}3_{SH1k}$-2_{NB10k}	3-arm, 1k	Linear, 10k	25	0.3
$P_{20}3_{SH1k}$-2_{NB20k}	3-arm, 1k	Linear, 20k	20	0.3
$P_{25}3_{SH1k}$-2_{NB20k}	3-arm, 1k	Linear, 20k	25	0.3
$P_{20}4_{SH2k}$-2_{NB6k}	4-arm, 2k	Linear, 6k	20	0.05
$P_{25}4_{SH2k}$-2_{NB6k}	4-arm, 2k	Linear, 6k	25	0.05
$P_{20}4_{SH2k}$-2_{NB10k}	4-arm, 2k	Linear, 10k	20	0.05
$P_{25}4_{SH2k}$-2_{NB10k}	4-arm, 2k	Linear, 10k	25	0.05
$P_{20}4_{SH2k}$-2_{NB20k}	4-arm, 2k	Linear, 20k	20	0.05
$P_{25}4_{SH2k}$-2_{NB20k}	4-arm, 2k	Linear, 20k	25	0.05
$P_{20}4_{SH2k}$-4_{NB20k}	4-arm, 2k	4-arm, 20k	20	0.05
$P_{25}4_{SH2k}$-4_{NB20k}	4-arm, 2k	4-arm, 20k	25	0.05

[a]The hydrogel naming (P_wX_{SHz}-Y_{NBz}) denotes the structure of the hydrogel. With W = polymer content (wt%), X = number of arms of PEO-thiol macromer, Y = number of arms of PEO-norbornene macromer, and Z = molecular weight of the PEO precursor.

S2: Schematic representation hydrogel mold. Dimensions in millimeters (mm).

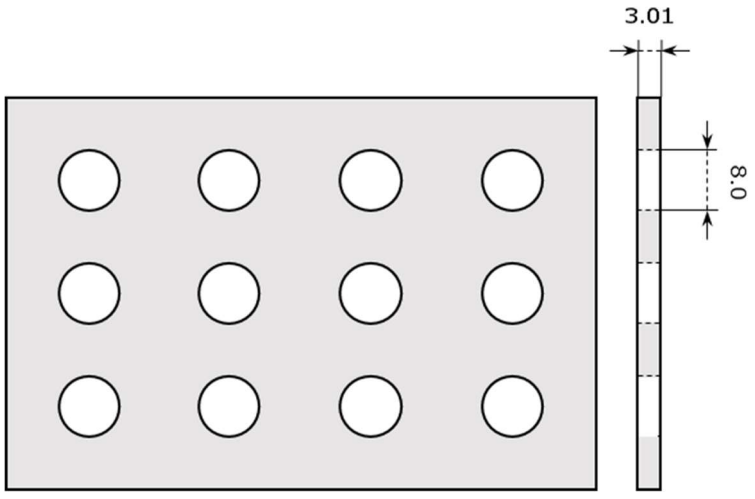

S3: Flory-Rehner calculations: hydrogel equilibrium swelling

EXPERIMENTAL

The mass swell ratio (Q_m) was calculated (eq. 4).

$$Q_m = \frac{m_{swollen}}{m_{dry}} \quad (4)$$

The volume swell ratio (Q_v) was calculated based on (Q_v) (eq. 5).

$$Q_v = 1 + \frac{\rho_p}{\rho_s}(Q_m - 1) \quad (5)$$

With ρ_p the polymer density (1.12 g/cm^3 for PEG), and ρ_s the solvent density (1 g/cm^3 for water). The average molecular weight between crosslinks ($\overline{M_c}$) was calculated as follows (eq. 5).

$$\frac{1}{\overline{M_c}} = \frac{2}{\overline{M_n}} = \frac{\frac{\bar{v}}{V_1}(\ln(1 - v_2) + v_2 + x_1 v_2^2)}{v_2^{\frac{1}{3}} - \frac{v_2}{2}} \quad (6)$$

With $\overline{M_n}$ the number average molecular weight of the un-crosslinked hydrogel (theoretical molecular weight of the polymer between crosslinks), V_1 the molar volume of the solvent (18 cm^3/mol for water), v_2 the polymer volume fraction in the equilibrium swollen hydrogel ($1/Q_v$), $\bar{v}$ the specific volume of the polymer (ρ_p/ρ_s), and x_1 the polymer-solvent interaction parameter (0.426 for PEO-water). Next, the $\overline{M_c}$ was used to calculate the crosslinking density (ρ_c) (eq. 6).

$$\rho_c = \frac{1}{\bar{v}\overline{M_c}} \quad (7)$$

The mesh size was then determined. First, the root-mean-square end-to-end distance of the polymer chain in the unperturbed state $(\bar{r}_0^2)^{\frac{1}{2}}$ was calculated (eq. 7).

$$(\bar{r}_0^2)^{\frac{1}{2}} = l C_n^{\frac{1}{2}} n^{\frac{1}{2}} \quad (8)$$

With l the average bond length (0.146 nm), $C_n$the characteristic ratio of the polymer (4.0 for PEO), and n the number of bonds in the crosslink (eq. 8).

$$n = 2\frac{\overline{M_c}}{M_r} \quad (9)$$

With M_r the molecular weight of the repeat unit (44.05 g/mol for PEO). Lastly, the mesh size (ξ) was calculated (eq. 9).

$$\xi = v_2^{-\frac{1}{3}}(\bar{r}_0^2)^{\frac{1}{2}} \quad (10)$$

S4: Flory-Rehner calculations: the ideal thiol-ene hydrogel network

THEORETICAL

The ideal or perfectly crosslinked thiol-ene hydrogel network without defects can be estimated by means of hydrogel equilibrium swelling. Considering the molecular weight and number of functionalities of the macromere building blocks, the $\overline{M_c}$ is defined as (eq. 10)

$$\overline{M_c} = 2\left(\frac{Mw_a + Mw_b}{f_a + f_b}\right) \quad (11)$$

With Mw_a and Mw_b the molecular weight of norbornene functionalized PEO (PEO-NB) and thiol functionalized PEO (PEO-SH) respectively. f_a and f_b are the number of reactive functionalities for PEO-NB and PEO-SH. With a known $\overline{M_c}$, the ideal crosslinking density or density of elastically active chains (v_c) and polymer volume fraction (v_2) can be calculated based on the Flory-Rehner theory (eq. 11)

$$v_c = \frac{V_1}{\overline{M_c}\,\overline{v_2}} = \frac{-(\ln(1 - v_2) + v_2 + x_1 v_2^2)}{v_2^{\frac{1}{3}} - \frac{2v_2}{f_a}} \quad (12)$$

With $\overline{v_2}$ the specific volume of PEO (0.92 cm^3/g at 37 °C). With $\overline{v_2}$, the ideal hydrogel mass swelling ratio ($Q_{m\ eq,\ ideal}$), can be calculated (eq. 12)

$$Q_{m\,eq,ideal} = \frac{(1 - v_2)\overline{v_2}}{\overline{v_1} v_2} + 1 \quad (13)$$

With $\overline{v_1}$ the specific volume of water (1.006 cm^3/g at 37 °C).

S5: ^{1}H-NMR spectra of functionalized poly(ethene oxide) (PEO)

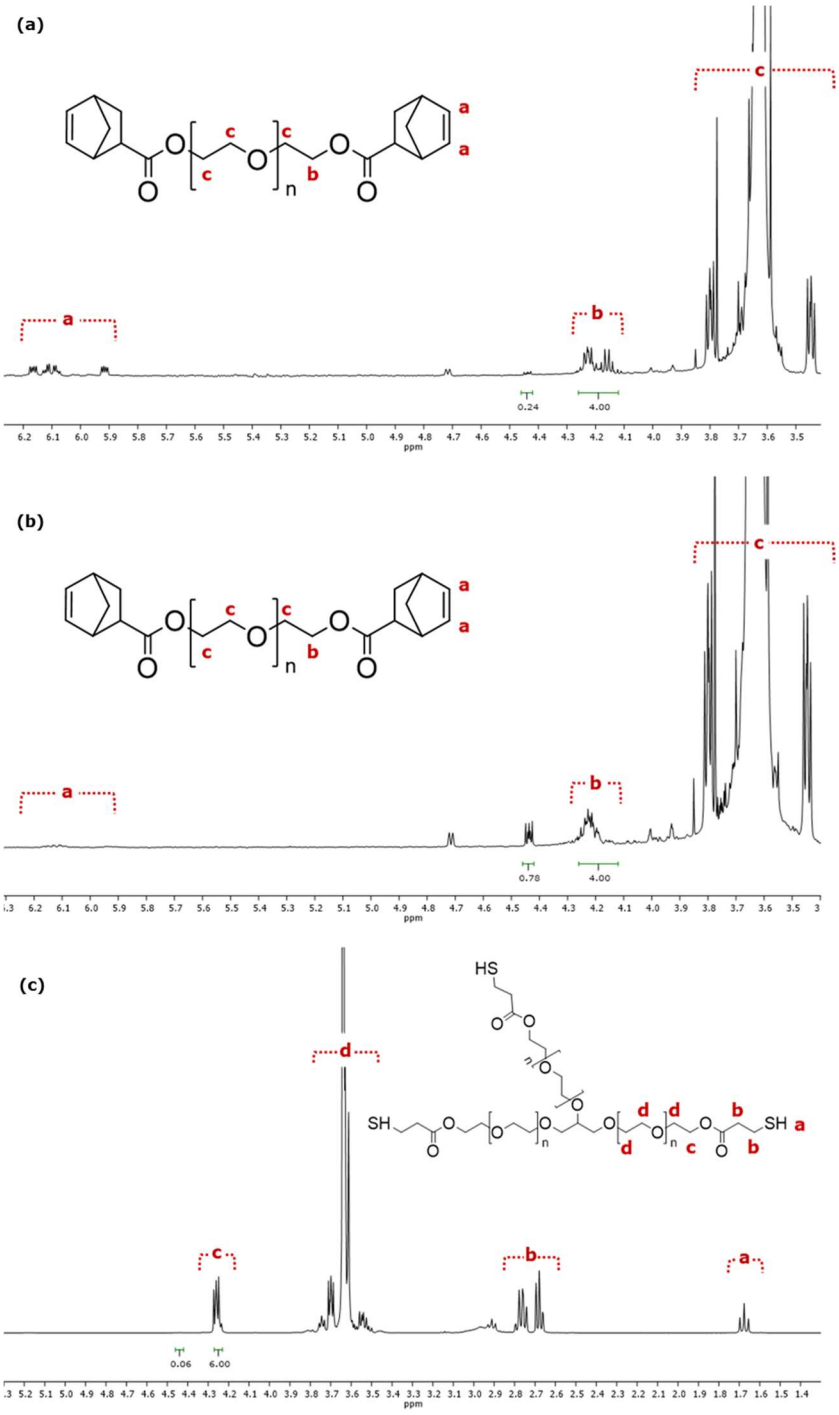

^{1}H-NMR (500 MHz, $CDCl_3$) shows quantitative thiol and norbornene end-functionalization of PEO based on the comparison of the theoretically expected protons next to the functionalized end-groups, to those of the unfunctionalized PEO. (a) Linear PEO norbornene (10k), 94% conversion. δ 4.12 – 4.26 (protons next to norbornene functionalized end-group, 2H per arm), δ 4.42 – 4.46 (protons next to unfunctionalized hydroxyl PEO end-group, 2H per arm), δ 6.19 – 5.90 (alkene protons from norbornene, 2H per arm). (b) Linear PEO norbornene (20k), 81% conversion. δ 4.12 – 4.26 (protons next to norbornene functionalized end-group, 2H per arm), δ 4.42 – 4.46 (protons adjacent to unfunctionalized hydroxyl PEO end-group, 2H per arm), δ 6.19 – 5.90 (alkene protons from norbornene, 2H per arm). (c) three-arm PEO thiol (1k), 99% conversion. δ 4.12 – 4.26 (protons next to thiol functionalized end-group, 2H per arm), δ 4.42 – 4.46 (protons adjacent to unfunctionalized hydroxyl PEO end-group, 2H per arm)

S6: Pictures cylindrical hydrogel samples for compression testing (a) $P_{20}3_{SH1k}$-2_{NB6k} (b) $P_{25}4_{SH2k}$-2_{NB10k}

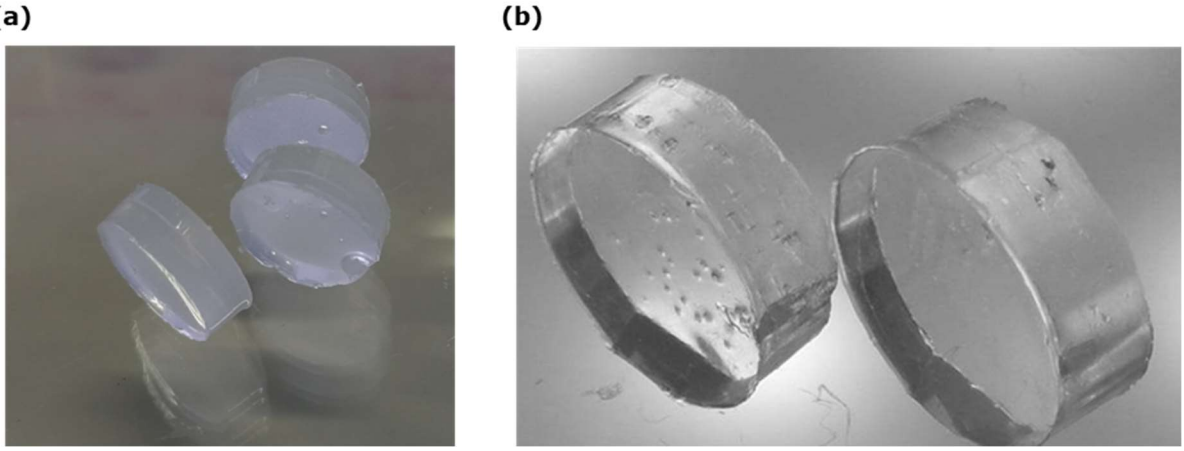

S7: Mechanical characterization of all hydrogel compositions

Hydrogel[a]	Average maximum stress (σ_{max}; MPa)	Average elastic modulus[b] (E; kPa)	Average toughness (AUC; MJ/m^3)
$P_{20}3_{SH1k}$-2_{NB6k}	2.2±0.1	178±21	26±3
$P_{20}3_{SH1k}$-2_{NB10k}	3.3±0.2	127±2	30±2
$P_{20}3_{SH1k}$-2_{NB20k}	3.5±0.1	121±5	32±1
$P_{25}3_{SH1k}$-2_{NB10k}	3.5±0.1	144±9	32±1
$P_{25}3_{SH1k}$-2_{NB20k}	3.4±0.1	108±3	33±1
$P_{20}4_{SH2k}$-2_{NB6k}	6.4±0.2	463±7	84±3
$P_{20}4_{SH2k}$-2_{NB10k}	4.3±0.1	241±14	50±2
$P_{20}4_{SH2k}$-2_{NB20k}	4.6±0.2	207±4	51±2
$P_{25}4_{SH2k}$-2_{NB6k}	6.6±0.1	564±8	90±2
$P_{25}4_{SH2k}$-2_{NB10k}	5.8±0.1	341±8	75±1
$P_{25}4_{SH2k}$-2_{NB20k}	4.7±0.1	208±2	52±1
$P_{20}4_{SH2k}$-4_{NB20k}	13.3±1.2	593±2	149±6
$P_{25}4_{SH2k}$-4_{NB20k}	16.4±0.6	895±10	190±6

[a]The hydrogel naming (P_wX_{SHz}-Y_{NBz}) denotes the structure of the hydrogel. With W = polymer content (wt%), X = number of arms of PEO-thiol macromer, Y = number of arms of PEO-norbornene macromer, and Z = molecular weight of the PEO precursor. [b]Calculated between 5-25% strain

S8: swelling behavior of hydrogels made with building blocks with increasing functionalities

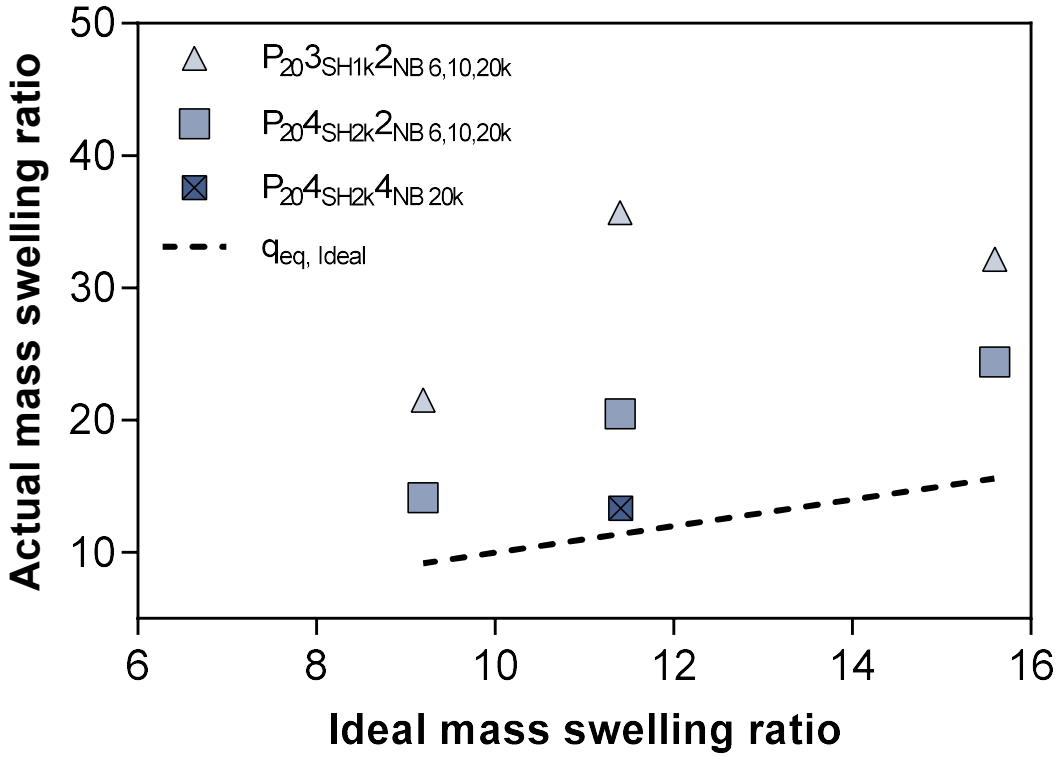

S9: Effect of LAP concentration on mechanical strength of $P_{20}4_{SH2k}$-2_{NB10} hydrogels

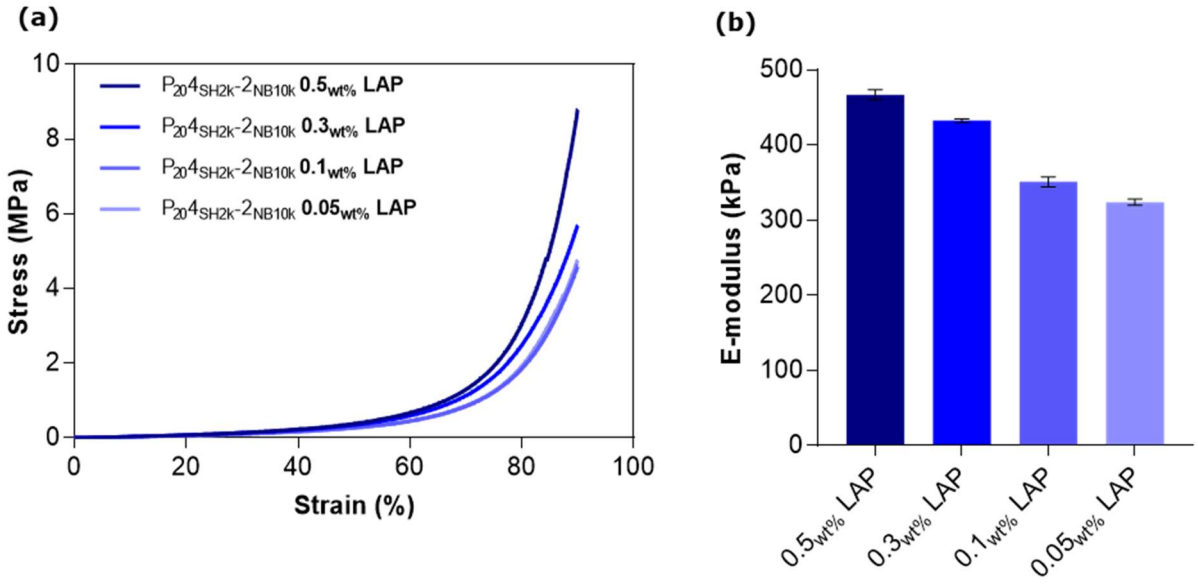

S10: Stress-strain curves of non-swollen, 24h and equilibrium (48h) swollen hydrogels

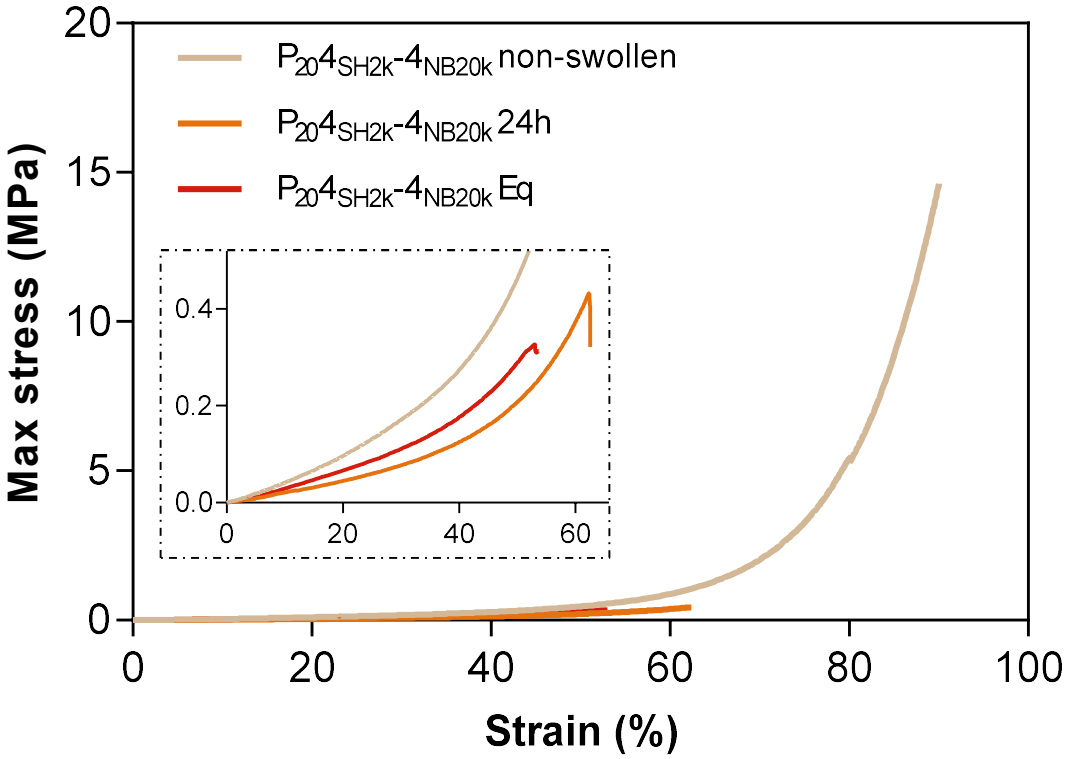

S11: DLP printed PEO hydrogel using 0.05 wt% LAP

(a) **(b)**